

2007

# A pseudo-rigid-body model for spherical mechanisms: The kinematics and elasticity of a curved compliant beam

Alejandro LeÃ³n

University of South Florida

Follow this and additional works at: <http://scholarcommons.usf.edu/etd>

 Part of the [American Studies Commons](#)

## Scholar Commons Citation

LeÃ³n, Alejandro, "A pseudo-rigid-body model for spherical mechanisms: The kinematics and elasticity of a curved compliant beam" (2007). *Graduate Theses and Dissertations*.  
<http://scholarcommons.usf.edu/etd/2259>

This Thesis is brought to you for free and open access by the Graduate School at Scholar Commons. It has been accepted for inclusion in Graduate Theses and Dissertations by an authorized administrator of Scholar Commons. For more information, please contact [scholarcommons@usf.edu](mailto:scholarcommons@usf.edu).

A Pseudo-Rigid-Body Model For Spherical Mechanisms: The Kinematics and Elasticity  
of a Curved Compliant Beam

by

Alejandro León

A thesis submitted in partial fulfillment  
of the requirements for the degree of  
Master of Science in Mechanical Engineering  
Department of Mechanical Engineering  
College of Engineering  
University of South Florida

Major Professor: Craig P. Lusk, Ph.D.  
Autar K. Kaw, Ph.D.  
Nathan Crane, Ph.D.

Date of Approval:  
November 6, 2007

Keywords: compliant mechanisms, large deflection, virtual work,  
mems, out of plane

© Copyright 2007 , Alejandro León

## **Dedication**

To my wife, Kathryn

## **Acknowledgements**

I wish to express my gratitude to everyone who contributed to making this thesis a reality. First, I'm specially grateful to my advisor Dr. Craig P. Lusk who patiently guided me and took me under his wing from the beginning to bring this thesis to fruition. He is a true role model. I also want to thank my committee members Dr. Nathan Crane and Dr. Autar K. Kaw for taking the time to read and provide me with feedback to improve this thesis. I would like to thank my brother, Hector León, for all of his guidance and advice through out my life you have made me a better man and have indirectly prepared me to tackle challenges like this thesis. Moreover, I would like to thank my parents, whom have loved me and supported me all my life, I love you guys so much, thank you. Additionally, I would like to thank my friend and lab mate, Joseph Chouiefati, you have been essential in keeping me motivated and without your shoulder to lean on, this thesis would have been much more difficult, thank you. Finally, I would like to thank the Mechanical Engineering Department., the College of Engineering and University of South Florida, Tampa Florida.

## Table of Contents

List of Tables .....	iii
List of Figures .....	iv
Abstract .....	vi
Chapter 1. Introduction .....	1
1.1 Objective .....	1
1.2 Motivation .....	2
1.3 Scope .....	2
1.4 Contributions .....	3
1.5 Roadmap .....	3
Chapter 2. Background .....	5
2.1 Pseudo-Rigid-Body .....	5
2.2 Kinematic portion for a Pseudo-Rigid-Body Model .....	6
2.3 Elastic portion for a Pseudo-Rigid-Body Model .....	8
Chapter 3. Methodology and Model Development .....	9
3.1 Correspondence between spherical and planar PRBMs .....	9
3.2 Model description of kinematics of compliant curved beam .....	10
3.3 Spherical Pseudo-Rigid-Body Model kinematics .....	13
3.4 Finite Element Model .....	15
3.5 Pseudo-Rigid-Body Model parameters .....	17
Chapter 4. Elastic Portion of a PRBM for a Spherical Mechanism .....	22
4.1 Introduction .....	22
4.2 Principle of virtual work .....	22
4.3 Stiffness Coefficient for a Spherical Pseudo-Rigid-Body Model .....	26
Chapter 5. Spherical PRBM Stress Analysis .....	29
5.1 Introduction .....	29
5.2 Development of bending stress for a spherical PRBM .....	30
5.3 Axial stress development for a spherical PRBM .....	32
5.4 Displacement constraint .....	33
5.5 Maximum Stress Analysis .....	35
Chapter 6. Results and Discussion .....	37
6.1 Kinematic improvements .....	37

6.2 Elastic portion .....	39
6.3 Stress analysis .....	40
6.4 Conclusion .....	41
References.....	42
Appendices.....	45
Appendix A: DETC paper .....	46
Appendix B: ANSYS batch code.....	57
Appendix C: MATLAB code.....	64
Appendix D: Napier's rule for spherical triangles .....	77

## List of Tables

Table 1	Position and orientation of coordinate frames .....	12
---------	---	----

## List of Figures

Figure 2.1	A PRBM link for a cantilever beam .....	6
Figure 2.1a	Cantilever segment with vertical force at the free end .....	7
Figure 2.1b	The PRBM equivalent.....	7
Figure 3.1	Reference frames describing the motion of the end of a compliant circular cantilever beam.....	11
Figure 3.2	Spherical mechanism with its respective kinematic definitions .....	13
Figure 3.3	The Pseudo-Rigid-Body Model of the compliant curved beam .....	15
Figure 3.4	Determination of error in the deflection approximation .....	18
Figure 3.5	The characteristic radius factor, $\gamma$ , versus the arc angle of the compliant beam, $\lambda$ .....	20
Figure 3.6	The parametric angle coefficient, $c_\theta$ , versus the arc angle of the compliant beam, $\lambda$ .....	21
Figure 3.7	The parameterization limit $\Theta_{\max}$ as a function of the arc angle subtended by the circular compliant beam, $\lambda$ .....	21
Figure 4.1	Spherical PRBM equivalent.....	24
Figure 4.2	$K_m$ , $K_f$ versus Lambda.....	28
Figure 5.1	Three-dimensional stress element at point P .....	29
Figure 5.2	$f_{cl}$ versus $\Theta$ for variable $\lambda$ and aspect ratio 0.1 .....	34
Figure 5.3	$f_{cl}$ versus $\Theta$ for variable $\lambda$ and aspect ratio 0.4.....	34
Figure 5.4	$f_{cl}$ versus $\Theta$ for variable $\lambda$ and aspect ratio 0.7 .....	35

Figure 6.1	The characteristic radius factor, $\gamma$ , versus the arc angle of the compliant beam, $\lambda$ .....	37
Figure 6.2	The parametric angle coefficient, $c_\theta$ , versus the arc angle of the compliant beam, $\lambda$ .....	38
Figure 6.3	The parameterization limit $\Theta_{\max}$ as a function of the arc angle subtended by the circular compliant beam, $\lambda$ .....	38
Figure 6.4	$\Theta_{\max}(K)$ versus Lambda.....	39
Figure 6.5	$K_m, K_f$ versus Lambda.....	40

# **A Pseudo-Rigid-Body Model For Spherical Mechanisms: The Kinematics and Elasticity of a Curved Compliant Beam**

Alejandro León

## **ABSTRACT**

This thesis improves a previous kinematic analysis and develops the elastic portion of the analysis of a curved compliant beam. This analysis is used to develop a Pseudo-Rigid-Body Model for the curved compliant beam. The Pseudo-Rigid-Body Model consist of kinematic and elastic parameters which can be used to simplify the computation of the large deflections of the beam as it undergoes spherical motion. The kinematic parameters that are developed are the characteristic radius,  $r$ , the parametric angle coefficient,  $c_\theta$ , and the kinematic parametrization limit,  $\Theta_{\max}(\gamma)$ . The elastic parameters developed are the stiffness coefficient,  $K_\theta$ , and the elastic parameterization limit,  $\Theta_{\max}(K)$ . Additionally, curve fit parameters are developed which enable the calculation of the stress in curved beam as it deflects

## **Chapter 1**

### **Introduction**

“What are the possibilities of small but movable machines? They may or may not be useful, but they surely would be fun to make.” [4]. In 1959, physicist Richard Feynman challenged researchers to explore the possibilities of technological advancement on the small scale. Since that time, computers have been reduced from room-size to desktop and hand-held devices, facilitated by ever-shrinking microelectronics. Micro-Electromechanical Systems (MEMS) fulfill Feynman’s vision. Notable among these is Texas Instrument’s DMD (Digital Mirror Device; an array of micro-mirrors, each acting as a single pixel), which is used in some computer projectors. Other examples, are pressure sensors and accelerometers, which are used in applications such as automotive airbags [5]. The integration of compliant mechanisms into MEMS fabrication stands to make a contribution in the design and performance of MEMS

#### **1.1 Objective**

The objective of this thesis was to develop the elastic parameters for a spherical Pseudo-rigid-body Model to expedite and simplify the analysis and design of compliant mechanisms. In addition, to develop the supporting software codes for finite element analysis (FEA) and the analysis of the FEA data.

## 1.2 Motivation

Most mechanisms are systems of levers, cams and gears, which move, rotate, and have rigid parts. On the other hand, *compliant mechanisms* are mechanisms that “gain some or all of their ability to move from the deflection of flexible segments” [1].

Compliant mechanisms may have improved performance and lower cost when compared with rigid-body mechanisms [2, 3]. Hence, the ability to expedite and simplify the analysis and design of compliant mechanisms could prove beneficial to designers. An area where the benefits could be greatly implemented would be in MEMS fabrication. MEMS can benefit a great deal in integrating compliant mechanisms in their designs. The use of compliant mechanisms allows MEMS to be easily fabricated, eliminates the use of hinges, allows for precise motion control, and practically eliminates wear [7].

## 1.3 Scope

Compliant mechanism theory permits a procedure called rigid-body replacement, in which two or more rigid links of the mechanism are replaced by a compliant flexure with equivalent motion [7]. Methods for designing flexures with equivalent motion to replace rigid links are detailed in Pseudo-Rigid-Body Models (PRBMs). In several texts, [16,22], rigid-body analysis and synthesis techniques have been classified as planar, spherical or spatial according to the type of vector algebra used to describe the mechanisms. In a planar mechanism, the path of any single part of a link lies in a plane and in a spherical mechanism, the path of any single part of a link lies on the surface of a sphere [17]. Numerous PRBMs have been developed for planar mechanisms [1, 9, 12, 13, 20] and used to design compliant mechanisms in applications such as prosthetics [25], clutches [26, 27], micro-bearings [28], and bistable mechanisms [29]. Thus, extensive

research has been done on planar compliant mechanisms using planar PRBMs. For MEMS applications that require mechanisms which rotate out-of-plane of fabrication, such as the Texas Instrument's DMD with an in-plane rotational input, or that rotate spatially about a point, spherical mechanisms may prove appropriate [18]. It is believed that the description of PRBMs for spherical compliant mechanisms will facilitate the design of MEMS with out-of-plane motion. In this thesis, a PRBM for a spherical compliant mechanism is developed. The kinematics of a curved flexure with the equivalent of a vertical end load have been described and the elastic parameters of the PRBM have been developed.

#### **1.4 Contributions**

This thesis has four major contributions to the analysis and design of compliant mechanisms. First, improvements to the PRBM kinematics developed by Jagirdar [17] were made. Where a robust form for calculating the y-axis rotational displacement,  $\phi$ , was developed, thus permitting a calculation of the horizontal angle  $\alpha$ . Second, the development of the elastic parameters for the PRBM of a spherical compliant mechanism. Thirdly, a FEA analysis was performed to validate the PRBM. As a result an ANSYS batch code had to be developed in order to allow large load steps runs for each aspect ratio of the compliant beam. Finally, a MATLAB code had to be developed in order to analyze the data produced by the FEA analysis.

#### **1.5 Roadmap**

This chapter has served as a general introduction to the work done in this thesis. Chapter 2 will introduce the background for PRBMs and the spherical kinematics. Chapter 3 will describe the analogy between a planar PRBM and a spherical PRBM and

detail the improvements made to Jagirdar [17]. Also, the FEA nomenclature, constraints used in the PRBM and its results will be presented. Chapter 4 will discuss the principle of virtual work and how it was coupled with the PRBM to develop the stiffness coefficient,  $K_{\theta}$ . In addition, chapter 4 will discuss the derivation of the governing equations for the FEA analysis of  $K_{\theta}$ . Chapter 5 describes the stress calculation for the spherical compliant beam and the derivations of the rotation matrices needed for the stress calculations based on the FEA data. Finally, chapter 6 will discuss the conclusions based on the results.

## Chapter 2

### Background

#### 2.1 Pseudo-Rigid-Body

Closed-form solutions for large deflections in cantilever beams have been developed in the past in the form of elliptic integrals. While elliptic integrals offer closed-form solutions to large-deflection problems they are limited to relative simple geometries and loadings and their derivations are laborious. It was observed that in all large deflections of cantilever beams the path of the beam end is nearly circular, with a center of curvature at some point on the undeflected part of the beam. This observation serves as the catalyst that leads to the development of the pseudo-rigid body model (PRBM) which allows for the motion of the end of the cantilever beam to be accurately approximated.

The PRBM consists of diagrams and equations describing the motion and stiffness of a compliant member in terms of a rigid-link equivalent mechanism which has the same motion and stiffness for a known range of motion and to a known mathematical tolerance. A PRBM can be used to perform analysis (i.e. given a compliant flexure, its motion can be found by treating it as the rigid body) or design (given a particular desired motion, a rigid body mechanism that performs the motion can be found, and the PRBM can be used to convert that rigid-body mechanism into a compliant mechanism). Once the rigid-body analogue to a compliant segment has been identified, the kinematic and

elastic parameters of the PRBM are optimized and validated so that the PRBM's range of applicability and level of error is known and acceptable [17].

## 2.2 Kinematic portion for a Pseudo-Rigid-Body Model

The PRBM allows a simplification of the bending of a compliant beam, by having an equivalent rigid-body link rotate about a *characteristic pivot* located a distance  $\gamma l$  away from the free end of the beam, where  $\gamma l$  is the *characteristic radius* and  $\gamma$  is the *characteristic radius factor* [17]. The Pseudo-Rigid-Body Model includes the development of a *pseudo-rigid-body angle*,  $\Theta$ , which is the amount of rotation about the pseudo pivot as shown in Figure 2.1.

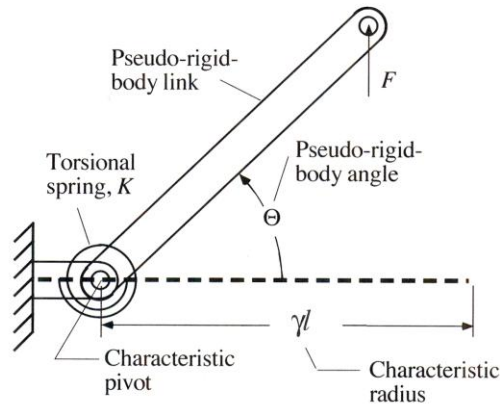


Figure 2.1 A PRBM link for a cantilever beam

The creation of such PRBMs is justified because they are easy to use in design and the use of the PRBM in connection with rigid-body synthesis techniques produces compliant mechanism configurations that are unlikely to be produced in any other way [17]. An example of a PRBM for a straight cantilever beam with vertical end load [7], is shown in Figure 2.2. Figure 2.2(a) shows a straight cantilever beam subjected to a vertical end load  $F$ . Figure 2.2(b) shows the pseudo-rigid-body equivalent of the straight cantilever

beam. The distance from the fixed end to the free end in the  $x$ -direction is  $a$ , the distance from the fixed end to the free end in the  $y$ -direction is  $b$ , length of the straight beam is  $l$ ,  $\Theta$  is the pseudo-rigid-body angle and  $\gamma$  is the characteristic radius factor. The angle of inclination of the beam at the beam end is given by  $\theta_0$ .

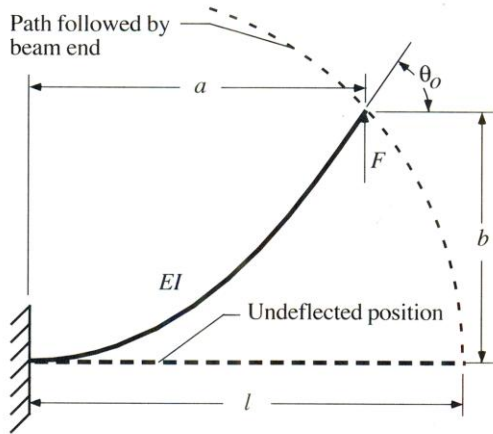


Figure 2.1a Cantilever segment with vertical force at the free end.

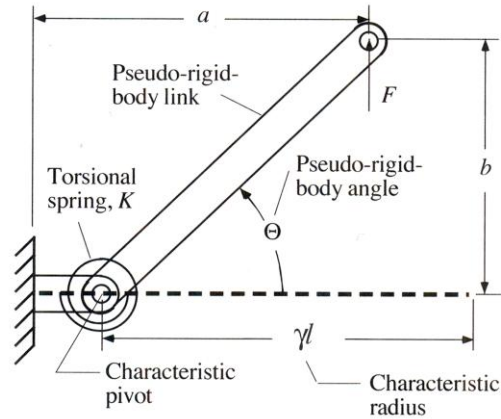


Figure 2.1b The PRBM equivalent

The coordinates of the beam end of the compliant beam are given in terms of the PRBM angle,  $\Theta$ , as:

$$a = l[1 - \gamma(1 - \cos \Theta)] \quad (2.1)$$

$$b = \gamma l \sin \Theta \quad (2.2)$$

Where  $\gamma=0.85$  for a vertical end load.

The relationship between  $\Theta$  and  $\theta_0$  is given by:

$$\theta_0 = 1.24\Theta \quad (2.3)$$

These relations are accurate to less than 0.5% error for  $\Theta < 64.3^\circ$ .

Howell's method [7] describes the criteria for calculating an acceptable value for the characteristic radius factor,  $\gamma$ , by first determining the maximum acceptable percentage error in deflection. The value for  $\gamma$  that would allow the maximum pseudo-rigid-body

angle,  $\Theta$ , while still keeping the error in the position of the beam end less than 0.5% can be calculated by:

$$\Theta = a \tan \frac{b}{a - l(1 - \gamma)} \quad (2.4)$$

As stated by [7, 9] and subject to the parametric constraint

$$g(\Theta) = \frac{\text{error}}{\varepsilon_e} \leq \left( \frac{\text{error}}{\varepsilon_e} \right)_{\max} \quad \text{for } 0 < \Theta < \Theta_{\max}(\gamma) \quad (2.5)$$

where  $\frac{\text{error}}{\varepsilon_e}$  is the relative deflection error, and  $\varepsilon_e$  is defined as the vector difference of the deflected position of point P and its original undeflected position.

### 2.3 Elastic portion for a Pseudo-Rigid-Body Model

The elastic portion of the PRBM includes a nondimensionalized torsional spring constant,  $K_{\Theta}$ , called the *stiffness coefficient*, to model the beam's resistance to deflection as shown on Figure 2.3. Combined with geometric and material properties, the stiffness coefficient is used to determine the value of the spring constant for a particular beam's pseudo-rigid-body model.  $K_{\Theta}$  facilitates the calculation of the force required to deflect the rigid-body system that is equivalent to the force needed to deflect the compliant beam [18]. The elastic portion also yields a  $\Theta_{\max}(K_{\Theta})$  for accurate force prediction.

An implicit advantage of the parametric approximation of the pseudo-rigid body model is that it can be used to obtain accurate initial estimates hence circumventing the laborious method of elliptic integrals.

## Chapter 3

### Methodology and Model Development

#### 3.1 Correspondence between spherical and planar PRBMs

In planar mechanisms, the joint axes are parallel; in spherical mechanisms, the joint axes intersect at the center of the sphere [16]. In planar compliant mechanisms, this characteristic is usually achieved by designing straight flexures that, at each point along their length are most flexible about parallel lines, and are considerably more rigid in other directions. In spherical compliant mechanisms, this characteristic can be achieved by designing curved flexures that, at each point along the arc, are most flexible about lines that point to the centre of the sphere. In both kinds of mechanisms, it is necessary that the length (arc-length) of the flexure be much greater than the width of the beam, and the width of the beam to be larger than its thickness [17]. It is hypothesized that a flexure which is a long, thin circular arc will move in a manner consistent with spherical kinematics when appropriately loaded [17].

There is a correspondence principle between spherical PRBMs and planar PRBMs. The correspondence principle is that when small angle assumption is used for spherical arcs. i.e. the arc length is much smaller than the radius of the sphere, the spherical PRBM becomes identical to planar PRBM. To emphasize the relationship between lines and arcs, in this thesis, the lengths in planar model are denoted with Roman letters, and the equivalent arcs in the spherical model are denoted with the Greek letter equivalents. For example the arc length,  $\beta$ , that appears in some formulas for spherical

mechanisms, can be related to the planar length,  $b$ . Thus, using small angle approximation:

$$\cos \beta = 1 \quad (3.1)$$

$$\sin \beta = \beta \rightarrow b \quad (3.2)$$

Where  $b$  is the planar equivalent of the arc  $\beta$ . Similarly  $a$  and  $l$  are the planar equivalent of arcs  $\alpha$  and  $\lambda$  respectively. Additionally, similar terminology is used in planar and spherical PRBMs, for angles between lines (arcs) such as  $\Theta, \theta_0$ , and for ratios such as  $\gamma$  and  $c_\theta$ . These variables do not change in the small angle case. In the planar case, the deflected angle of beam end,  $\theta_0$ , is about an axis normal to the plane. Similarly, in the spherical case, the deflection of the beam end,  $\theta_0$ , is about an axis normal to the tangent plane to the sphere at the beam end.

### 3.2 Model description of kinematics of compliant curved beam

In order to implement the PRBM some reference frames must first be identified. The following nomenclature was developed by Saurabh Jagirdar [17] for the implementation of the PRBM in the kinematic analysis of a compliant curved beam, and will further be used in this thesis for the kinetic analysis. The kinematics of the compliant circular cantilever,  $PQ$ , is described by using a series of coordinate frames, as shown in Figure 3.1.

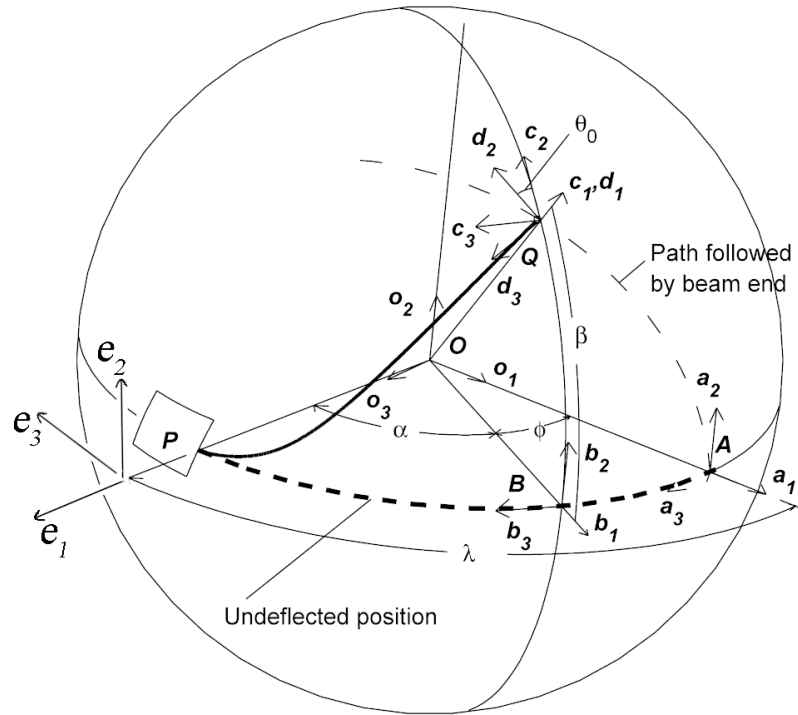


Figure 3.1 Reference frames describing the motion of the end of a compliant circular cantilever beam

The fixed end of the curved cantilever beam is denoted as  $P$  and free end of the beam as  $Q$ . Let the center of a sphere be defined by frame  $O$  and the frames  $A$ ,  $B$ ,  $C$  and  $D$  are on the surface of the sphere. The position and orientation of the coordinate frames are related as follows [18]:

Table 1 Position and orientation of coordinate frames

Frame	Frame Descriptions [17]
O	This frame is attached to the center of the sphere. The $O_1$ axis passes through the un-deflected beam end Q. The $O_2$ axis is normal to the plane containing the un-deflected beam. The $O_3$ axis completes the right-handed orthogonal triad and is parallel with the neutral axis of the un-deflected beam end at Q.
A	This frame has the same orientation as the O frame and is located at the end of the un-deflected beam.
B	This frame locates the deflected position of the beam end Q in the $a_1-a_3$ a plane (analogous to the translation in the x-direction in the planar model).
C	This frame describes movement of beam end Q in the $b_2-b_1$ plane rotating about point O (analogous to the translation in the y-direction in the planar model)
D	This frame is at the same position as the C frame and tracks the rotation of the beam end about the radial axis through the beam end (analogous to the rotation of the beam end about the z-axis in the planar model)
E	This frame describes relative position of beam end P with respect to the other frames

The frames are described by the matrices  $A$ ,  $B$ ,  $C$  and  $D$ , where the columns of the matrix are the basis vectors. The transformations relating the frames are given by:

$$A = [\{\hat{a}_1\}, \{\hat{a}_2\}, \{\hat{a}_3\}] = \begin{bmatrix} 1 & 0 & 0 \\ 0 & 1 & 0 \\ 0 & 0 & 1 \end{bmatrix} \quad (3.3)$$

$$B = [\{\hat{b}_1\}, \{\hat{b}_2\}, \{\hat{b}_3\}] = \begin{bmatrix} \cos(\phi) & 0 & -\sin(\phi) \\ 0 & 1 & 0 \\ \sin(\phi) & 0 & \cos(\phi) \end{bmatrix} A = R(\hat{a}_2, -\phi)A \quad (3.4)$$

$$C = [\{\hat{c}_1\}, \{\hat{c}_2\}, \{\hat{c}_3\}] = \begin{bmatrix} \cos(\beta) & -\sin(\beta) & 0 \\ \sin(\beta) & \cos(\beta) & 0 \\ 0 & 0 & 1 \end{bmatrix} B = R(\hat{b}_3, \beta)B \quad (3.5)$$

$$D = [\{\hat{d}_1\}, \{\hat{d}_2\}, \{\hat{d}_3\}] = \begin{bmatrix} 1 & 0 & 0 \\ 0 & \cos(\theta_0) & -\sin(\theta_0) \\ 0 & \sin(\theta_0) & \cos(\theta_0) \end{bmatrix} C = R(\hat{c}_1, \theta_0)C \quad (3.6)$$

Thus, the motion of the curved cantilever beam is described by the parameters  $\phi = \lambda - \alpha$ ,  $\beta$  and  $\theta_0$  which are analogous to planar parameters  $l-a$ ,  $b$  and  $\theta_0$ , respectively. These parameters are shown in Figure 3.1.

Moreover, an additional frame is needed for the elastic portion of the PRBM. Frame E which is located at a point P, typically is the point of highest bending stress.

$$E = [\{\hat{e}_1\}, \{\hat{e}_2\}, \{\hat{e}_3\}] = \begin{bmatrix} \cos(\alpha) & 0 & -\sin(\alpha) \\ 0 & 1 & 0 \\ \sin(\alpha) & 0 & \cos(\alpha) \end{bmatrix} B = R(\hat{b}_2, -\alpha)B \quad (3.7)$$

### 3.3 Spherical Pseudo-Rigid-Body Model kinematics

An example of the implementation of the PRBM for a spherical compliant mechanism can be seen in Figure 3.2 with its respective kinematic definitions.

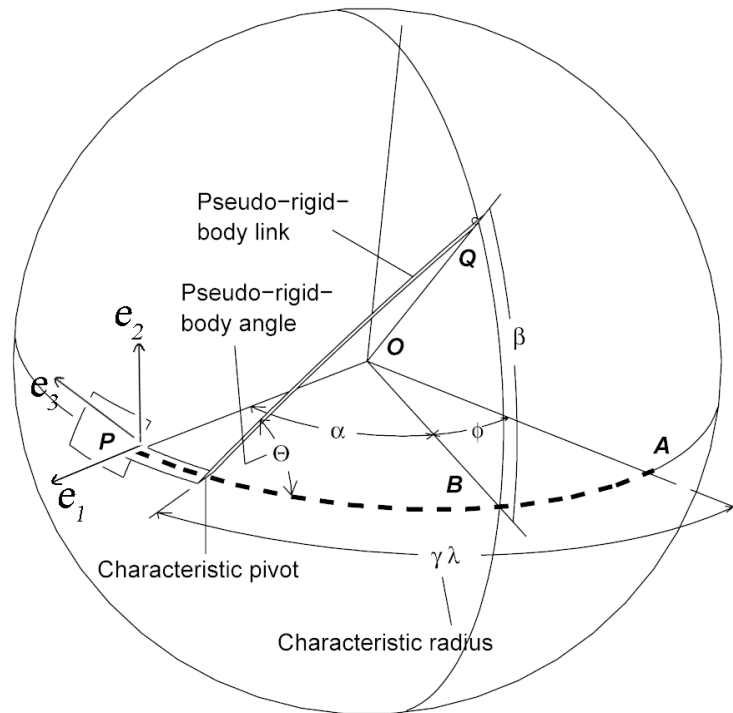


Figure 3.2 Spherical mechanism with its respective kinematic definitions

The angle  $\Theta$  is defined as the pseudo-rigid-body angle for both the planar and the spherical PRBMs. The characteristic radius factor,  $\gamma$ , is defined as the length from the beam end to the pseudo-pivot divided by the length of the beam. The compliant beam's neutral axis subtends an arc,  $\lambda$ , and its PRBM consists of two rigid links, which make up circular arcs of  $\gamma\lambda$  and  $(1-\gamma)\lambda$ , and are joined by a revolute joint which is located at center O [18].

The relationships for  $\alpha$  and  $\beta$  in terms of  $\gamma$  and  $\Theta$  are obtained using Napier's rules for right spherical triangles [19], on the triangle shown in Figure 3.2 with sides  $\gamma\lambda$ ,  $\gamma\lambda - \phi$ , and  $\beta$ . One finds, the y-axis rotational displacement,  $\phi$ , as a function of  $\gamma\lambda$  and  $\Theta$  as:

$$\phi = \tan^{-1} \left( \frac{[1 - \cos \Theta]}{\cot \gamma\lambda + \cos \Theta \tan \gamma\lambda} \right) \quad (3.7)$$

The horizontal angle  $\alpha$  :

$$\alpha = \lambda - \phi \quad (3.8)$$

The vertical angle  $\beta$  :

$$\beta = \sin^{-1}(\sin \gamma\lambda \sin \Theta) \quad (3.9)$$

Equations 3.7 and 3.8 are the result of improvements made to the PRBM kinematics for calculating  $\alpha$ , first developed by Jagirdar [17]. Equation 3.7 is a robust form for calculating  $\phi$  which removes singularities at  $\gamma\lambda = 90$ . Equation 3.8 then allows for the calculation of  $\alpha$  from  $\phi$ .

### 3.4 Finite Element Model

To compute the deflection of the curved beam undergoing spherical motion, the beam was modeled in a commercial FEA software package (ANSYS 11). Three-dimensional beam elements with six degrees-of-freedom (BEAM 4) were used. Because large deflection analysis was required, the iterative nonlinear solver was used. The loading conditions proved easiest to apply using the double slider model. A load was applied to the FEA model such that there is no reaction load at the fixed end,  $P$ , and the free end,  $Q$ , of curved cantilever beam moves in a manner consistent with spherical kinematics. The load direction depends on the displacement of the beam end, and the displacement of the beam end depends on the load direction. Thus, to ensure that there is no reaction load at the fixed end,  $P$ , we need to know the path followed by the beam end, as shown in

Figure 3.3.

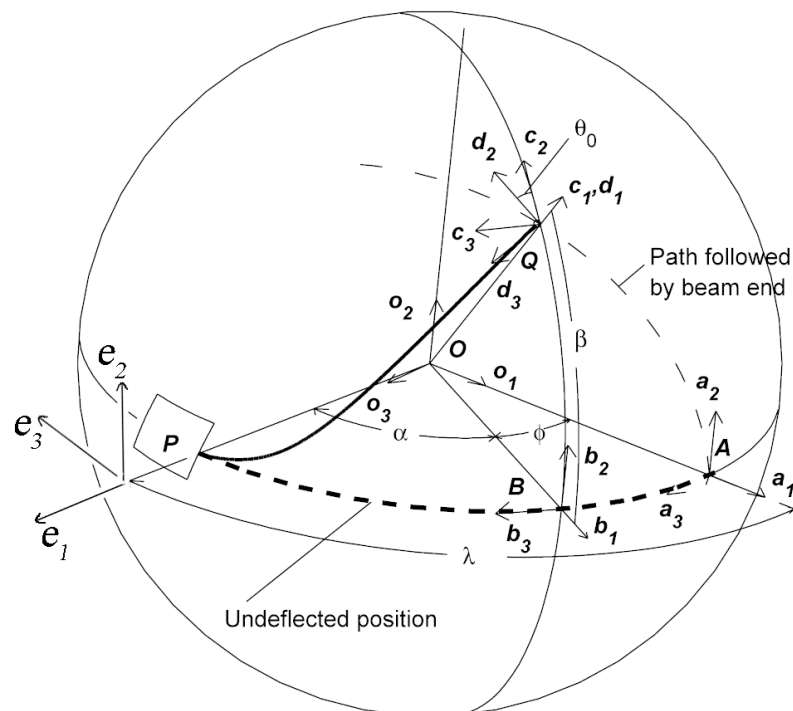


Figure 3.3 The Pseudo-Rigid-Body Model of the compliant curved beam

The path followed is an arc on the sphere from the A frame (undeflected position  $Q$ ) to the C or D frame (final position of  $Q$ ). When the beam  $PQ$  is taken as fixed at  $P$ , the A-frame of reference is fixed. The motion of the beam can also be described in the B-frame of reference such that the end  $Q$  of the beam is allowed to move in the  $b_1 - b_2$  plane only. Also, point  $Q$  was constrained to rotate an amount  $\beta$  about the  $O_3$  axis and was permitted to rotate freely about the  $O_1$  and  $O_2$  axes. Thus, the input parameter is the angle  $\beta$  which determines both the rotation of the beam end  $Q$  and its deflection. One output obtained is the rotation angle,  $\phi = \lambda - \alpha$ , of the beam end  $P$  as it moves along a circular arc in the  $b_1 - b_3$  plane (pure rotation about  $O_2$  axis). The other output is the rotation,  $\theta_0$ , of the neutral axis of the beam at  $Q$  about the radial axis. That is, the beam undergoes spherical motion such that the ends  $P$  and  $Q$  move on orthogonal great circles. The simulation was repeated varying:

- a) The initial beam angle  $\lambda$
- b) The aspect ratio of the curved flexible beam (thickness divided by width  $\frac{h}{b}$ )

Simulations were run for beam angles ranging from 4 degrees to 112 degrees in increments of one degree and aspect ratios of 0.1, 0.4, 0.7. The values of the input displacement,  $\beta$  were applied in 1600 even increments ranging from 0 degrees up to the beam angle  $\lambda$ . Additionally, in order to efficiently perform the simulation an ANSYS batch code was developed. The batch code allows the user to automatically cycle through all the different angles of  $\lambda$  and its corresponding aspect ratio. Otherwise, an user would be force to manually change  $\lambda$  and the aspect ratio for each run from 4 to 112 degrees. The parametric angle coefficient,  $c_\theta$ , the characteristic radius factor,  $\gamma$ , and the

parameterization limit,  $\Theta_{\max}(\gamma)$ , are obtained from the results of the FEA model using the procedure described in the next section. Additionally, the ANSYS code also calculated the force  $f_{c2}$  and the moment  $M$  for the elastic portion discussed in chapter 4.

### 3.5 Pseudo-Rigid-Body Model parameters

The development of the spherical PRBM kinematics lends itself to develop the corresponding PRBM parameters by following Howell's method [7]. An optimal value for the characteristic radius factor,  $\gamma$ , may be found given a maximum acceptable percentage error in deflection. Based on equations 3.7 and 3.8 we found the value of  $\gamma$  that would allow the maximum pseudo-rigid-body angle,  $\Theta_{\max}(\gamma)$ , while keeping the error in the position of the beam end less than 0.5 %. Napier's rules can be used to express the dependence of the pseudo-rigid-body angle,  $\Theta$ , on  $\gamma$  for the spherical PRBM. From [18] we have:

$$\sin \beta = \sin \Theta \sin \gamma \lambda \quad (3.10)$$

$$\cos \Theta = \tan(\gamma \lambda - \phi) \cot \gamma \lambda \quad (3.11)$$

Therefore,

$$\Theta = \tan^{-1} \left[ \frac{\sin \beta}{\tan(\gamma \lambda - \phi) \cos \gamma \lambda} \right] \quad (3.12)$$

which is subject to the parametric constraint

$$g(\Theta) = \frac{\text{error}}{\varepsilon_e} \leq \left( \frac{\text{error}}{\varepsilon_e} \right)_{\max} \quad (3.13)$$

where  $\frac{error}{\varepsilon_e}$  is the relative deflection error, and  $\varepsilon_e$  is defined as the vector difference of the deflected position of point Q and its original undeflected position. The deflection obtained using FEA,  $\varepsilon_e$ , is shown in Figure 3.4 and can be calculated from the beam motion parameters,  $\beta$  and  $\phi$  [18] as:

$$\varepsilon_e = R(b_3, \beta)R(a_2, -\phi)a_1 - a_1 = \begin{bmatrix} \cos \beta \cos \phi - 1 \\ \sin \beta \\ \cos \beta \sin \phi \end{bmatrix} \quad (3.14)$$

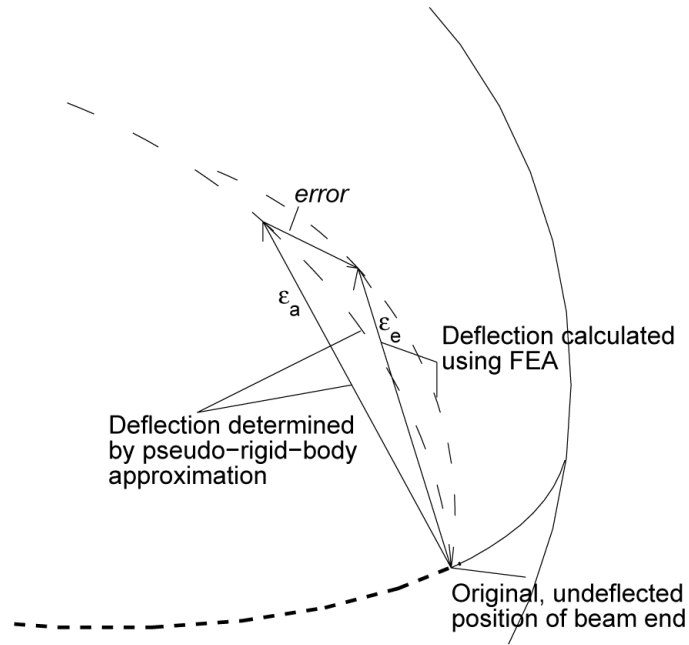


Figure 3.4 Determination of error in the deflection approximation

The PRBM deflection estimate,  $\varepsilon_a$ , is given by the vector difference of the deflected location of point Q calculated using the PRBM and its undeflected coordinates, or

$\vec{\varepsilon}_a = \vec{Q} - a_1$ . The position of point Q according to the PRBM is  $\vec{Q} = R\vec{a}_1$  where R is the

rotation operator that acts on the vector  $a_1$  and rotates it about the pseudo pivot,  $\vec{m}$ , through an angle  $\Theta$  [18]. The action of the operator R on  $a_1$  is given [30] by:

$$\vec{Q} = R\vec{a}_1 = (1 - \cos \Theta)(\vec{m} \cdot \vec{a}_1)\vec{m} + \cos \Theta \vec{a}_1 + \sin \Theta(\vec{m} \times \vec{a}_1) \quad (3.15)$$

where  $\vec{m} = \begin{bmatrix} \cos \gamma\lambda \\ 0 \\ \sin \gamma\lambda \end{bmatrix}$  and  $a_1 = \begin{bmatrix} 1 \\ 0 \\ 0 \end{bmatrix}$ , which reduces to

$$\vec{Q} = R\vec{a}_1 = \begin{bmatrix} \cos^2 \gamma\lambda(1 - \cos \Theta) + \cos \Theta \\ \sin \gamma\lambda \sin \Theta \\ \cos \gamma\lambda \sin \gamma\lambda(1 - \cos \Theta) \end{bmatrix} \quad (3.16)$$

Therefore [18],

$$\varepsilon_a = \begin{bmatrix} \cos^2 \gamma\lambda(1 - \cos \Theta) + \cos \Theta - 1 \\ \sin \gamma\lambda \sin \Theta \\ \cos \gamma\lambda \sin \gamma\lambda(1 - \cos \Theta) \end{bmatrix} \quad (3.17)$$

The *error* is defined as magnitude of the vector difference between the final positions of the curved flexible segment found using FEA and the final position found using the Pseudo-Rigid-Body Model with a particular value of  $\gamma$ . Thus, the *error* in the deflection is calculated as:

$$error = |\varepsilon_e - \varepsilon_a| = \sqrt{(\varepsilon_{ex} - \varepsilon_{ax})^2 + (\varepsilon_{ey} - \varepsilon_{ay})^2 + (\varepsilon_{ez} - \varepsilon_{az})^2} \quad (3.18)$$

The *relative error*, is defined as:

$$\frac{error}{\varepsilon_e} = \frac{|\vec{\varepsilon}_e - \vec{\varepsilon}_a|}{|\vec{\varepsilon}_e|} \quad (3.19)$$

Appendix C gives the MATLAB code for finding the parameterization limit  $\Theta_{\max}(\gamma)$ .

The procedure used MATLAB's interpolation functions to determine with accuracy the value of  $\Theta_{\max}(\gamma)$  at which the error in the model approximation exceeded 0.5%.

Furthermore, based on equations 3.7 and 3.8, refinements to the FEA code, and the use of MATLAB's interpolation functions (see Appendixes B and C), improvements in the calculations of parameters  $\gamma$ ,  $c_\theta$ , and  $\Theta_{\max}(\gamma)$  were made. Figures 3.4, 3.5, and 3.6 illustrate the improved calculations for  $\gamma$ ,  $c_\theta$ , and  $\Theta_{\max}(\gamma)$ , respectively, as well as for each aspect ratio.

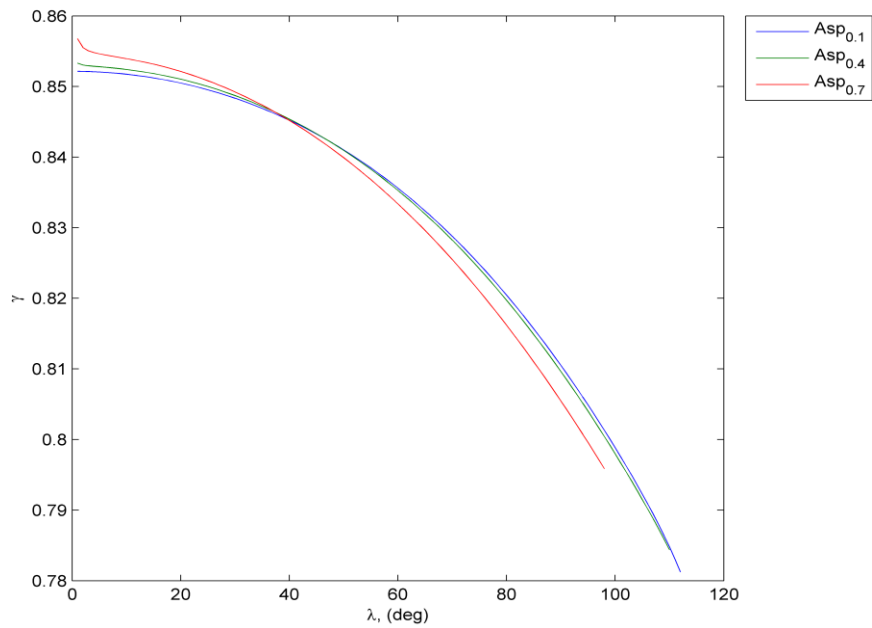


Figure 3.5 The characteristic radius factor,  $\gamma$ , versus the arc angle of the compliant beam,  $\lambda$ .

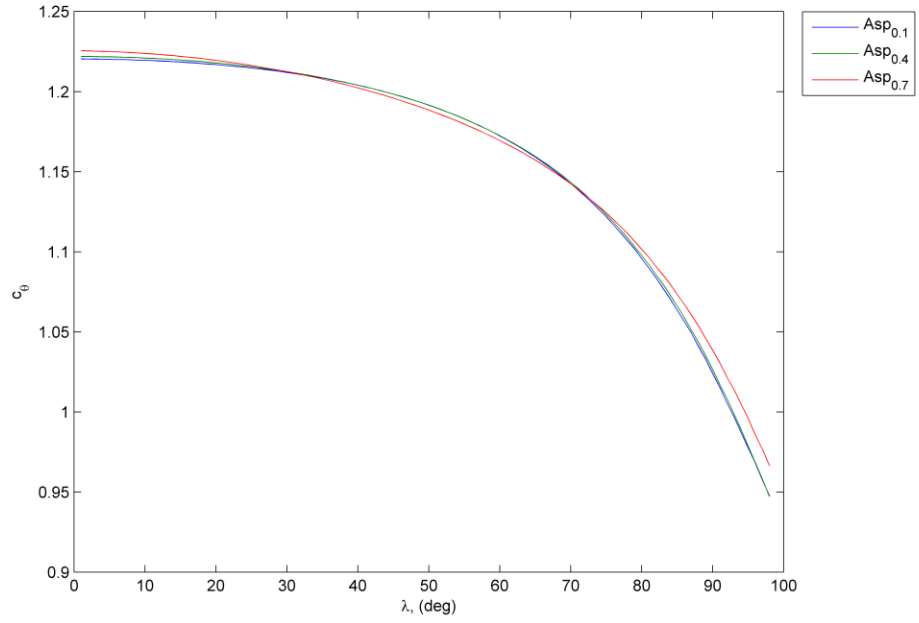


Figure 3.6 The parametric angle coefficient,  $c_{\theta}$ , versus the arc angle of the compliant beam,  $\lambda$ .

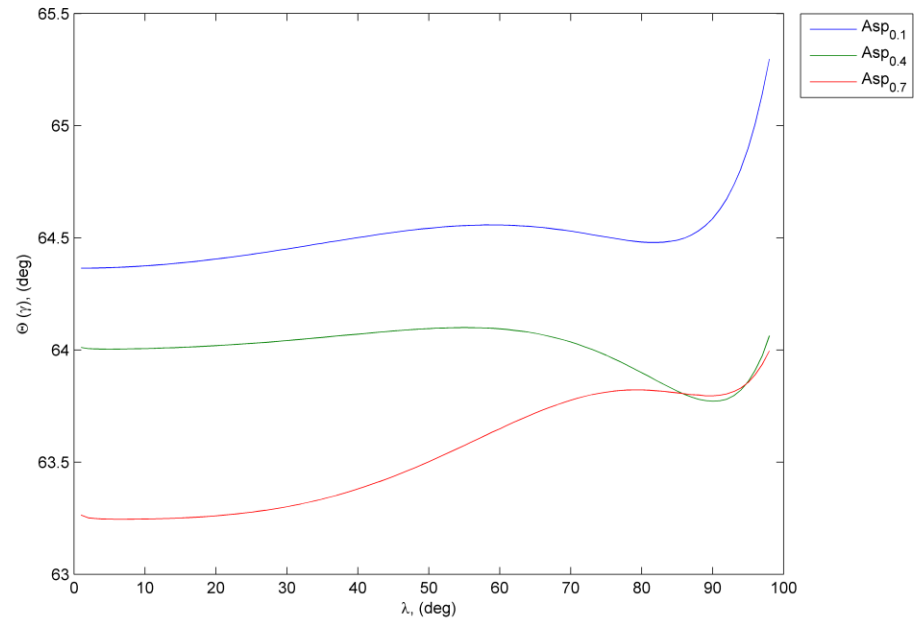


Figure 3.7 The parameterization limit  $\Theta_{\max}$  as a function of the arc angle subtended by the circular compliant beam,  $\lambda$ .

## Chapter 4

### Elastic Portion of a PRBM for a Spherical Mechanism

#### 4.1 Introduction

This thesis uses the principle of virtual work and the Pseudo-Rigid-Body Model concept to develop force-deflection relationships for compliant mechanisms. Why do we use virtual work, as oppose to the well known Newtonian approach? It is worth mentioning, that one of the main advantages of using the virtual work approach is that the system, in this case the spherical compliant mechanism, is viewed and analyzed from an energy perspective and thus the end-reaction forces are not necessary because they do not move and hence do no work, greatly simplifies the force-deflection analysis.

#### 4.2 Principle of virtual work

The principle of virtual work may be expressed as follows [21]: “The net virtual work of all active forces is zero if and only if an ideal mechanical system is in equilibrium.” An ideal mechanical system is one is which the constraints do no work where it can be expressed as  $\sum \delta W = 0$  . The compliant mechanism in this thesis will be assumed to be ideal.

In order to evaluate virtual work, a virtual displacement must first be considered. A virtual displacement is a small, arbitrary displacement,  $\delta \mathbf{x}$ , which is expressed as a

function of the generalized coordinates. The virtual work,  $\delta W$ , due to an applied force  $\vec{F}$ , and a virtual displacement,  $\delta \vec{z}$ , is:

$$\delta W = \vec{F} \cdot \delta \vec{z} \quad (4.1)$$

Similarly, the virtual work due to an applied moment,  $\vec{M}$ , and a virtual angular displacement,  $\delta \hat{\theta}$ , is:

$$\delta W = \vec{M} \cdot \delta \hat{\theta} \quad (4.2)$$

A force is conservative if the work done by the force is independent of path, that is, dependent on the coordinate of the displacement endpoints only [7]. In this case, the work done is the difference in the potential energy,  $V$ , of the system at the two endpoints:

$$W = V_1 - V_2$$

The work done on a spring fits this category. The strain energy of a spring may be determined from

$$V = \int_{s_0}^s f_k(s) ds \quad (4.3)$$

where  $f_k(s)$  is the spring force as a function of  $s$  and  $s_0$  is the value of  $s$  for which the spring force is zero.

Torsional springs are also common in pseudo-rigid-body models, and their strain energy may be calculated in general form as:

$$V = \int_{\psi_0}^{\psi} m_k(\psi) d\psi \quad (4.4)$$

where  $m_k(\psi)$  is the spring torque as a function of  $\psi$  and  $\psi_0$  is the value of  $\psi$  for which the spring torque is zero. The PRBM in this thesis uses a linear spring. The general nonlinear forms of equations (4.3) and (4.4) are [7]:

$$\delta W = -f_k(s) \frac{ds}{dq} \delta q \quad (4.5)$$

$$\delta W = -m_k(\psi) \frac{d\psi}{dq} \delta q \quad (4.6)$$

This form is useful because integration and differentiation of the nonlinear spring functions are avoided. It is important to note that with a virtual work approach the number of generalized coordinate must be equal to the number of degrees of freedom of the system. The number of equations is also equal to the number of degrees of freedom [7]. The force-displacement characteristics of the compliant mechanism in this thesis were found by applying the principle of virtual work. The following derivations are provided in the context of the Pseudo-Rigid-Body Model of the compliant mechanism in Figure 4.1.

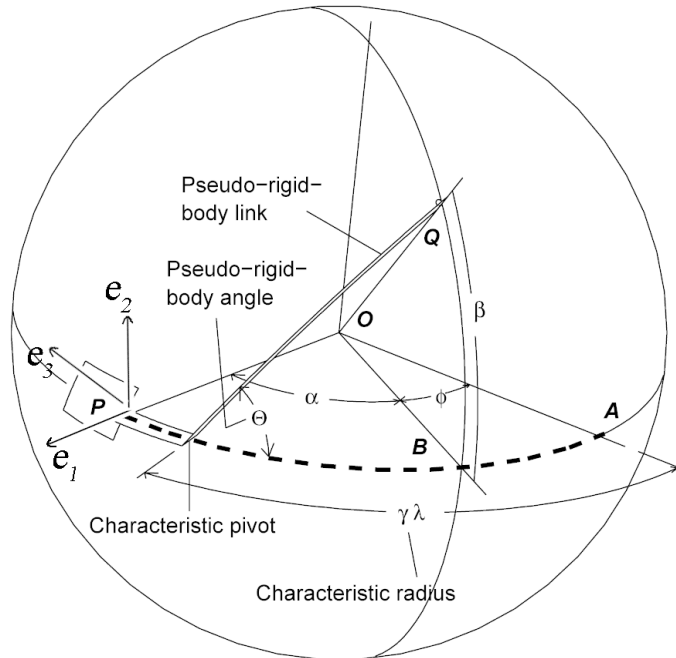


Figure 4.1 Spherical PRBM equivalent

A force,  $f_{c2}$ , was applied parallel to the  $\hat{c}_2$  at the end point Q, an output moment, M, about  $\hat{c}_3$  and a linear torsional spring to represent a small-length flexural pivot at  $\gamma\lambda$  with a

spring constant of  $K$  . In this thesis, the force  $f_{c2}$ , and the moment  $M$  were calculated using an ANSYS batch code as described in chapter 3 (see Appendix B). In order to apply the principle of virtual work, the input rotation,  $\beta$  , was chosen as the generalized coordinate. Next we write the force  $f_{c2}$ , and  $M$  in vector form as:

$$\vec{f}_{c2} = (f_{b1} R \sin \beta) \hat{b}_1 + (f_{b2} R \cos \beta) \hat{b}_2 \quad (4.7)$$

$$\vec{M} = M_{c3} \cdot \delta\beta \quad (4.8)$$

The virtual displacement,  $\delta_z$  , is found by writing a vector,  $\vec{Z}$  , from a fixed point, the origin, to the placement of each force, as follows:

$$\vec{Z} = (R \cos \beta) \hat{i} + (R \sin \beta) \hat{j} + 0 \hat{k} \quad (4.9)$$

Next the virtual displacement was found by differentiating the position vector  $\vec{Z}$  with respect to the generalized coordinate,  $\beta$  .

$$d\vec{z} = (-R \sin \beta \hat{i} + R \cos \beta \hat{j}) \delta\beta \quad (4.10)$$

The virtual work due to the force  $f_{c2}$ , was calculated by taking the dot product of the force vector and the virtual displacement. The virtual work due to the moment  $\vec{M}$  , was added to the virtual work done by the applied force  $f_{c2}$ . Equation 4.11 is the result.

$$\delta W = \vec{f}_{c2} \cdot \delta\vec{z} + \vec{M} \cdot \delta\beta = (-f_{b1} R \sin \beta + f_{b2} R \cos \beta + M_{c3}) \delta\beta \quad (4.11)$$

Until this point we have accounted for the virtual work done by the applied forces and the moments, but we have yet to take into account the virtual work done by the spring. In the next section we will look at the virtual work done by the spring and how it is derived.

### 4.3 Stiffness Coefficient for a Spherical Pseudo-Rigid-Body Model

The PRBM offers the ability to model a compliant beam's resistance to bending. The beam's resistance to deflection may be modeled by a nondimensionalized torsional spring constant,  $K_{\Theta}$  called the *stiffness coefficient*. Combined with geometric and material properties, the stiffness coefficient is used to determine the value of the spring constant,  $K$ , for a particular beam's Pseudo-Rigid-Body Model [7]. To calculate  $K_{\Theta}$  the principle of virtual work in conjunction with the PRBM concept is used to develop force-deflection relationships for compliant mechanisms as outlined in [20].

Moreover, the PRBM in this thesis includes a linear spring to model the stiffness of the beam and quantify its opposition to  $f_{c2}$ . From equation 4.6 and as shown in [7]

$m_k(\psi) = K\psi$  and letting  $\psi = \Theta$  the spring's virtual work equals:

$$\delta W = -K\Theta \frac{d\Theta}{d\beta} \delta\beta \quad (4.12)$$

where  $\frac{d\Theta}{d\beta}$  is found using Napier's rules for spherical triangles [19] as follows:

For  $\beta < 90^\circ$

$$\sin \beta = \sin \Theta \sin \gamma\lambda \quad (4.12a)$$

taking the derivative  $\frac{d\beta}{d\Theta}$  of equation 4.12a yields:

$$\cos \beta \frac{d\beta}{d\Theta} = \cos \Theta \sin \gamma\lambda \quad (4.12b)$$

solving for  $\frac{d\beta}{d\Theta}$  and taking the reciprocal:

$$\frac{d\Theta}{d\beta} = \frac{\cos \Theta \sin \gamma\lambda}{\cos \beta} \quad (4.12c)$$

Thus, the total virtual work of the system is the sum of all the virtual work components:

$$\delta W_{Total} = (-f_{\bar{b}1} R \sin \beta + f_{\bar{b}2} R \cos \beta + M_{\bar{c}3} - K_{\Theta} \frac{d\Theta}{d\beta}) \delta\beta = 0 \quad (4.13)$$

where  $K = K_{\Theta} \frac{\lambda R}{EI}$  and substituting into equation 4.13 we can then solve for the parameter of interest. In this case  $K_{\Theta}$ .

$$K_{\Theta} = \frac{d\beta}{d\Theta} \left[ \frac{-f_{\bar{b}1} R \sin \beta + f_{\bar{b}2} R \cos \beta + M_{\bar{c}3}}{\Theta} \right] \cdot \frac{\lambda R}{EI} \quad (4.14)$$

where  $\frac{\lambda R}{EI}$  is a nondimensionalization factor. We further separate  $K_{\Theta}$  into its contributing components  $K_m$  (the stiffness contributed by the moment) and  $K_f$  (the stiffness contributed by the force  $f_3$ ) and graph them with respect to  $\lambda$ , where

$$K_f = \left( \frac{f_{\bar{b}1} R \sin \beta}{\Theta} + \frac{f_{\bar{b}2} R \cos \beta}{\Theta} \right) \frac{d\beta}{d\Theta} \cdot \frac{\lambda R}{EI} \quad (4.15)$$

$$K_m = \frac{M_{\bar{c}3}}{\Theta} \frac{d\beta}{d\Theta} \cdot \frac{\lambda R}{EI} \quad (4.16)$$

as seen in Figure 4.2.

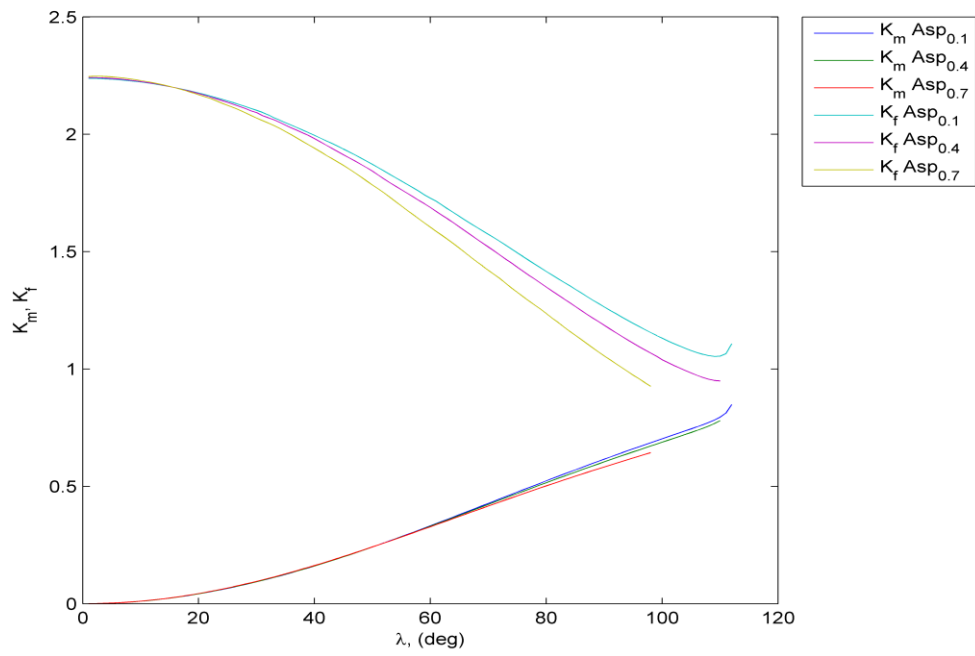


Figure 4.2  $K_m$ ,  $K_f$  versus Lambda

## Chapter 5

### Spherical PRBM Stress Analysis

#### 5.1 Introduction

One of the most critical aspects of compliant mechanism design is ensuring that the mechanism will undergo its specified task without failing [7]. To this end, the stress analysis for the spherical PRBM has been developed. In any mechanism, the area most likely to fail is the area that experiences maximum stress. For the curved compliant beam point P is the point of maximum stress. Figure 5.1 shows a three-dimensional stress element with its axes  $\hat{e}_1, \hat{e}_2, \hat{e}_3$  aligned with side, top and frontal axis of the beam, respectively at point P. The vertical shear forces,  $V_{e1}$  and  $V_{e2}$ , shown on Figure 5.1 make a negligible contribution to the overall stress at point P, thus will not be included in the stress analysis.

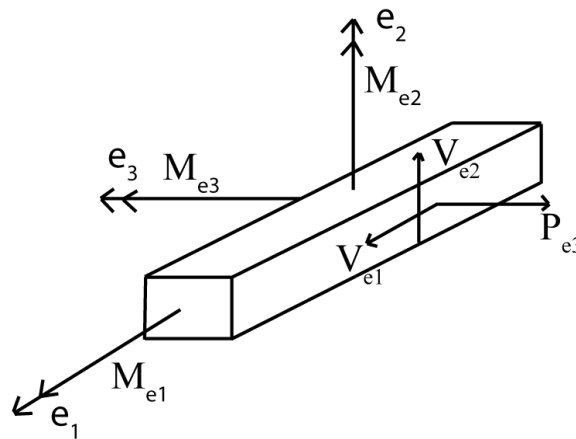


Figure 5.1 Three-dimensional stress element at point P

## 5.2 Development of bending stress for a spherical PRBM

As shown on Figure 5.1, point P experiences several different forces and moments that cause stress; in this section, the stress caused by moments  $M_{e_1}$ ,  $M_{e_2}$  and  $M_{e_3}$  are calculated. An additional frame, E, was developed in order to locate and describe the movement of point P, as shown in equation 3.7. Restated for reference:

$$E = [\{\hat{e}_1\}, \{\hat{e}_2\}, \{\hat{e}_3\}] = \begin{bmatrix} \cos(\alpha) & 0 & -\sin(\alpha) \\ 0 & 1 & 0 \\ \sin(\alpha) & 0 & \cos(\alpha) \end{bmatrix} B = R(\hat{b}_2, -\alpha)B \quad (5.1)$$

In order to calculate the moment at P caused by a force at frame C, several frame transformations took place. First, the position vector  $\vec{r}$  locates point Q with respect to point P, and was developed as follows:

$$\vec{r} = Q - P = R[\cos \beta \hat{b}_1 + \sin \beta \hat{b}_2] - R[\cos \alpha \hat{b}_1 + \sin \alpha \hat{b}_3] \quad (5.2)$$

where substituting for the unit vectors  $\hat{b}_1, \hat{b}_2, \hat{b}_3$ , given by equation 3.5, with respect to frame C into equation 5.2 yields:

$$\vec{r} = R \begin{bmatrix} (\cos \beta - \cos \alpha) \cos \beta + \sin^2 \beta \\ -(\cos \beta - \cos \alpha) \sin \beta + \sin \beta \cos \beta \\ -\sin \alpha \end{bmatrix} \quad (5.3)$$

equation 5.3 simplifies to:

$$\vec{r} = R \begin{bmatrix} 1 - \cos \beta \cos \alpha \\ \cos \alpha \sin \beta \\ -\sin \alpha \end{bmatrix} \quad (5.4)$$

then to describe the moment at P caused by a force at C with respect to frame C we take  $\vec{r} \times \vec{f}$  where  $\vec{f}$  is calculated from the ANSYS code and will be taken in the general form of

$$\vec{f} = f_1\hat{c}_1 + f_2\hat{c}_2 \quad (5.5)$$

thus the  $\vec{r} \times \vec{f}$  yields an expression of the moment at P caused by a force at C, with respect to frame C as follows:

$${}^cM_p = \vec{r} \times \vec{f} = \begin{bmatrix} \hat{c}_1 & \hat{c}_2 & \hat{c}_3 \\ r_1 & r_2 & r_3 \\ f_1 & f_2 & 0 \end{bmatrix} = -r_3f_2\hat{c}_1 + r_3f_1\hat{c}_2 + (r_1f_2 - r_2f_1)\hat{c}_3 + M\hat{c}_3$$

$${}^cM_p = \begin{bmatrix} Rf_2(\sin \alpha) \\ -Rf_1(\sin \alpha) \\ (Rf_2(1 - \cos \beta \cos \alpha) - Rf_1(\cos \alpha \sin \beta) + M_{c3}) \end{bmatrix} \quad (5.6)$$

Similarly, a moment at P caused by a force at C with respect to frame B:

$${}^cM_p = (R \sin \alpha) f_2 [\cos \beta, \sin \beta, 0]^T - (R \sin \alpha) f_1 [-\sin \beta, \cos \beta, 0]^T + R(1 - \cos \beta \cos \alpha) f_2 - R(\cos \alpha \sin \beta) f_1 + M_{c3} [0, 0, 1]^T \quad (5.7)$$

multiplying through and rearranging equation 5.7 yields:

$${}^cM_p = (f_2 R \sin \alpha \cos \beta + f_1 R \sin \alpha \sin \beta) \hat{b}_1 + (f_2 R \sin \alpha \sin \beta - f_1 R \sin \alpha \cos \beta) \hat{b}_2 + (Rf_2(1 - \cos \beta \cos \alpha) - Rf_1(\cos \alpha \sin \beta) + M_{c3}) \hat{b}_3$$

writing  ${}^cM_p$  in a more compact form yields equation 5.8,

$${}^cM_p = \begin{bmatrix} R(f_2 \sin \alpha \cos \beta + f_1 \sin \alpha \sin \beta) \\ R(f_2 \sin \alpha \sin \beta - f_1 \sin \alpha \cos \beta) \\ (Rf_2(1 - \cos \beta \cos \alpha) - Rf_1(\cos \alpha \sin \beta) + M_{c3}) \end{bmatrix} \quad (5.8)$$

Finally, the moment at P caused by a force at C with respect to frame E

${}^cM_p = {}^cM_p \cdot {}^B M_p$  where  ${}^B M_p$  is the rotation about O described by equation 5.1, thus we

have:

$${}^cM_p = (Rf_2 \sin \alpha \cos \beta + Rf_1 \sin \alpha \sin \beta) [\cos \alpha, 0, -\sin \alpha] + (Rf_2 \sin \alpha \sin \beta - Rf_1 \sin \alpha \cos \beta) [0, 1, 0] + Rf_2(1 - \cos \beta \cos \alpha) - Rf_1(\cos \alpha \sin \beta) + M_{c3} [\sin \alpha, 0, \cos \alpha] \quad (5.9)$$

equation 5.9 simplifies to:

$${}^C_E M_P = \begin{bmatrix} (Rf_2(\sin \alpha) + M_{e_3}(\sin \alpha)) \\ R(f_2 \sin \alpha \sin \beta - f_1 \sin \alpha \cos \beta) \\ -(Rf_2(\cos \beta - \cos \alpha) - Rf_1 \sin \beta + M_{e_3}(\cos \alpha)) \end{bmatrix} \quad (5.10)$$

equation 5.10 shows the individual contribution of  $M_{e_1}$ ,  $M_{e_2}$  and  $M_{e_3}$  to the overall bending stress, hence:

$$M_{e_1} = (Rf_2(\sin \alpha) + M_{e_3}(\sin \alpha)) \quad (5.11)$$

$$M_{e_2} = R(f_2 \sin \alpha \sin \beta - f_1 \sin \alpha \cos \beta) \quad (5.12)$$

$$M_{e_3} = -(Rf_2(\cos \beta - \cos \alpha) - Rf_1 \sin \beta + M_{e_3}(\cos \alpha)) \quad (5.13)$$

where equation 5.13 can be seen as the torsion about the  $e_3$  axis.

### 5.3 Axial stress development for a spherical PRBM

The development for the axial stress is very similar to how the bending stress was derived in the previous section. As shown in Figure 5.1, point P experiences a load in the  $\hat{e}_3$  direction which creates an axial stress on the  $e_2$ - $e_1$  plane. The effects of the force at frame C on point P with respect to frame E were derived in a similar way as the bending stress. Starting with equation 5.5, where  $\vec{f} = f_1\hat{c}_1 + f_2\hat{c}_2$  and substituting for vectors  $\hat{c}_1$  and  $\hat{c}_2$  yields:

$$\vec{f} = \begin{bmatrix} (f_1 \cos \beta - f_2 \sin \beta) \\ (f_1 \sin \beta - f_2 \cos \beta) \end{bmatrix} \quad (5.14)$$

repeating the substitution process for vectors  $\hat{b}_1$  and  $\hat{b}_2$  using equation 5.1 yields:

$$\vec{f} = \begin{bmatrix} f_1 (\cos \beta \cos \alpha) - f_2 (\sin \beta \cos \alpha) \\ f_1 \sin \beta + f_2 \cos \beta \\ -f_1 (\cos \beta \sin \alpha) + f_2 (\sin \beta \sin \alpha) \end{bmatrix} \quad (5.15)$$

equation 5.15 shows the individual contribution of  $V_{e1}$ ,  $V_{e2}$  and  $P_3$  to the overall axial stress, hence:

$$V_{e1} = f_1 (\cos \beta \cos \alpha) - f_2 (\sin \beta \cos \alpha) \quad (5.16)$$

$$V_{e2} = f_1 \sin \beta + f_2 \cos \beta \quad (5.17)$$

$$P_3 = -f_1 (\cos \beta \sin \alpha) + f_2 (\sin \beta \sin \alpha) \quad (5.18)$$

#### 5.4 Displacement constraint

An important parameter that emerges from the analysis of this spherical compliant mechanism is that a force  $f_{c1}$  is necessary for the mechanisms to remain in spherical motion. This is not a working force (e.g doesn't cause displacement), thus it was not taking into account for the elastic parameter calculations, but it contributes to the stress at point P. Force  $f_{c1}$  was plotted for several different beam angles  $\lambda$  and the parametric angle  $\Theta$  to better study the stress in the beam and its spherical motion. Figures 5.3, 5.4, and 5.5 are the graphs of  $f_{c1}$  for aspect ratio 0.1, 0.4, and 0.7 respectively.

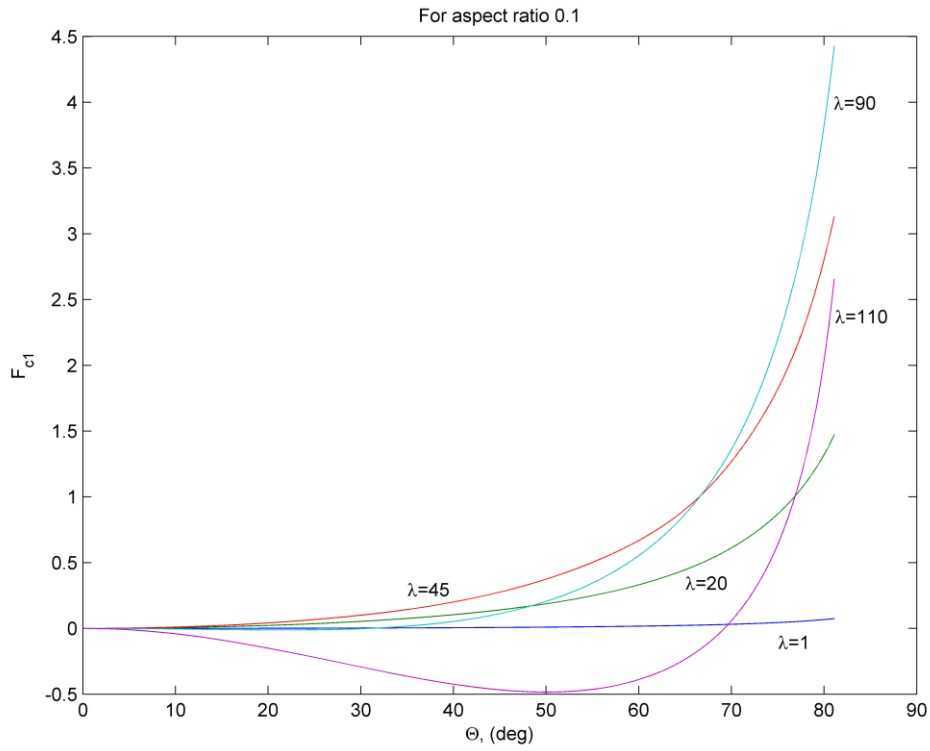


Figure 5.2  $f_{c1}$  versus  $\Theta$  for variable  $\lambda$  and aspect ratio 0.1

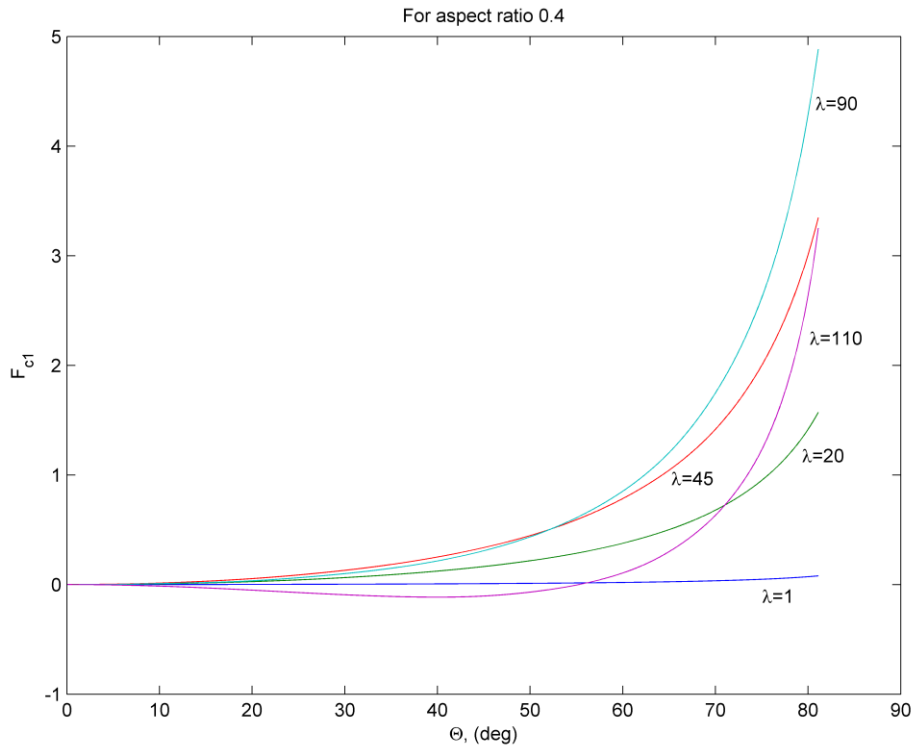


Figure 5.3  $f_{c1}$  versus  $\Theta$  for variable  $\lambda$  and aspect ratio 0.4

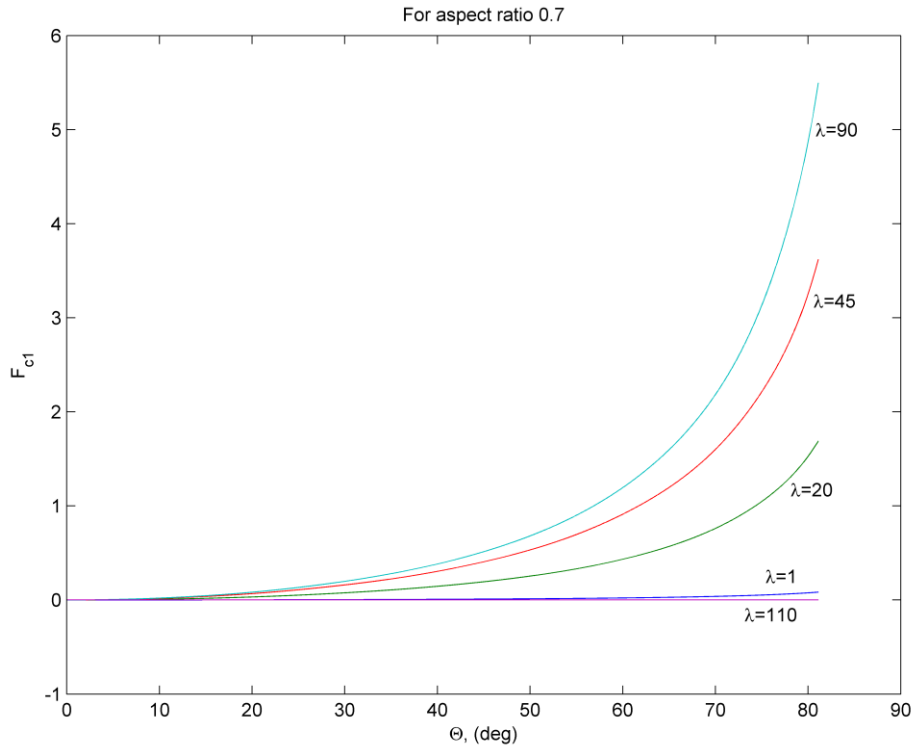


Figure 5.4  $f_{c1}$  versus  $\Theta$  for variable  $\lambda$  and aspect ratio 0.7

### 5.5 Maximum Stress Analysis

Maximum stress at point P can be summed in the following way:

$$\sigma_{\max} = \frac{M_{e1} \cdot c_{e1}}{I_{e1}} + \frac{M_{e2} \cdot c_{e2}}{I_{e2}} + \frac{P_3}{A} \quad (5.19)$$

$$\tau_{\max} = \frac{M_{e3} \cdot \alpha \cdot b}{JG} \quad (5.20)$$

where  $I$  is the second moment of area about the neutral axis,  $c$  is the location of the centroid of the beam and  $A$  is the area of the cross-section of the beam, hence:

$$\sigma_{\max} = \begin{bmatrix} (Rf_2(\sin \alpha) + M_{e3}(\sin \alpha)) \frac{c_{e1}}{I_{e1}} \\ R(f_2 \sin \alpha \sin \beta - f_1 \sin \alpha \cos \beta) \frac{c_{e2}}{I_{e2}} \\ -(Rf_2(\cos \beta - \cos \alpha) - Rf_1 \sin \beta + M_{e3}(\cos \alpha)) \frac{c_{e3}}{I_{e3}} \end{bmatrix} + \left( \frac{-f_1(\cos \beta \sin \alpha) + f_2(\sin \beta \sin \alpha)}{A} \right)$$

## Chapter 6

### Results and Discussion

#### 6.1 Kinematic improvements

The spherical PRBM allows that for a given value of aspect ratio,  $\frac{h}{b}$ , and beam angle,  $\lambda$ , one can find a value of characteristic radius factor,  $\gamma$ , and parametric angle coefficient,  $c_\theta$ , that best approximates the motion (position and orientation of beam at various input displacements) up to the parameterization limit,  $\Theta_{\max}(\gamma)$ . Moreover, improvements to previous work done by Jagirdar in the calculations of parameters  $\gamma$ ,  $c_\theta$ , and  $\Theta_{\max}(\gamma)$  were made. Figures 6.1, 6.2, and 6.3 illustrate the improved calculations for  $\gamma$ ,  $c_\theta$ , and  $\Theta_{\max}$ , respectively, as well as for each aspect ratio.

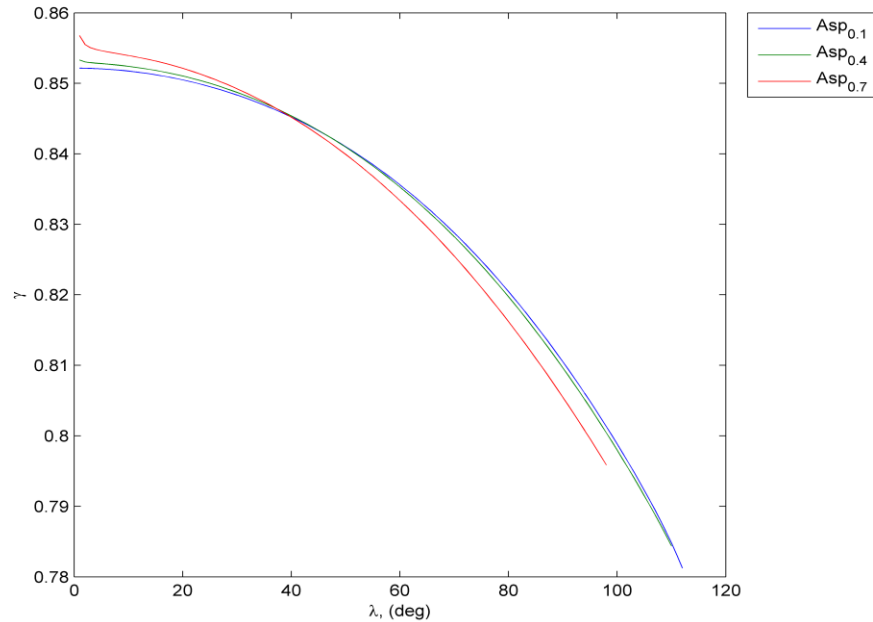


Figure 6.1 The characteristic radius factor,  $\gamma$ , versus the arc angle of the compliant beam,  $\lambda$ .

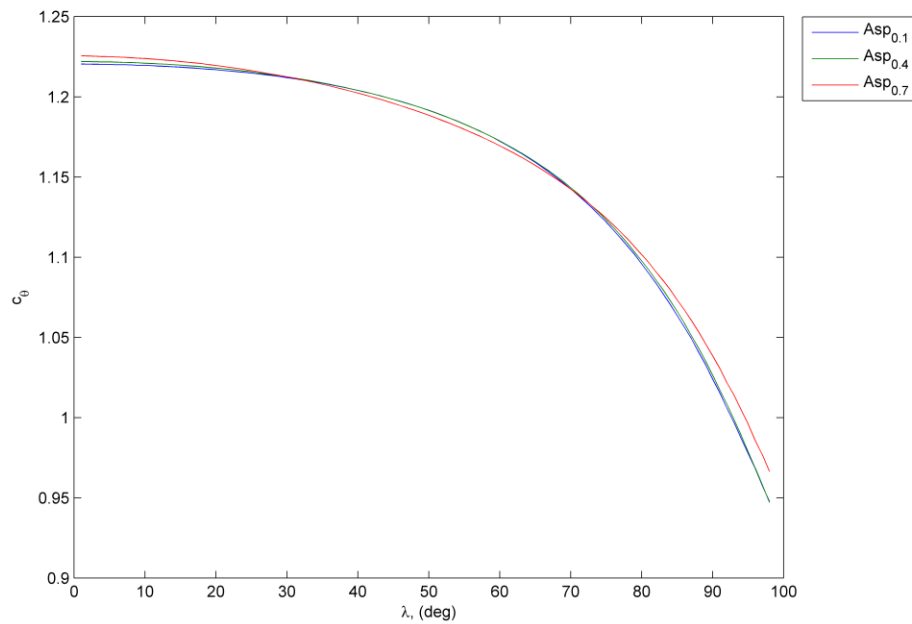


Figure 6.2 The parametric angle coefficient,  $c_\theta$ , versus the arc angle of the compliant beam,  $\lambda$ .

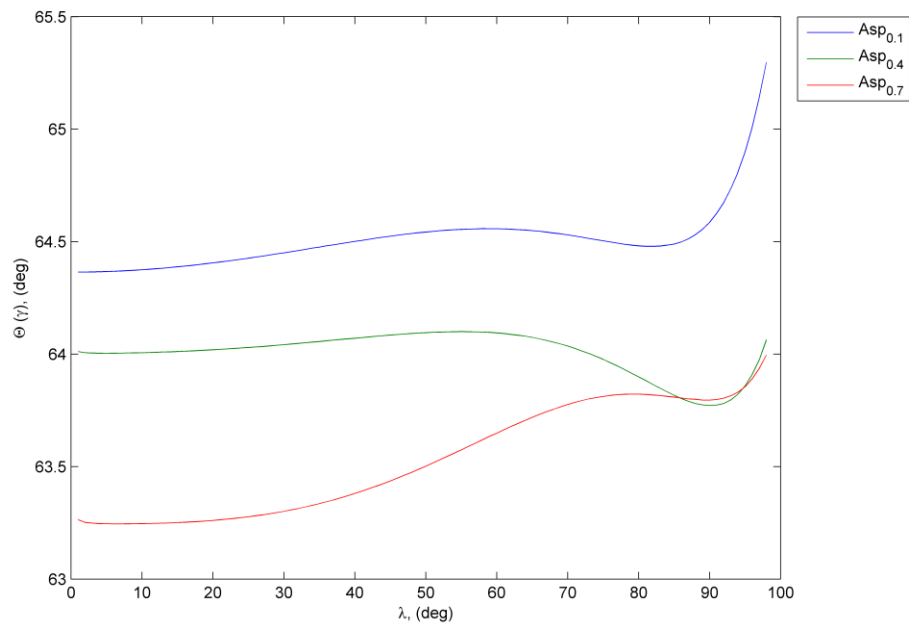


Figure 6.3 The parameterization limit  $\Theta_{max}$  as a function of the arc angle subtended by the circular compliant beam,  $\lambda$ .

## 6.2 Elastic portion

In addition, for a given value of aspect ratio,  $\frac{h}{b}$ , and beam angle,  $\lambda$ , and characteristic radius factor,  $\gamma$ , one can find a value for the stiffness coefficient,  $K_{\Theta}$ , that best approximates the motion (position, orientation and stiffness of a beam at various input displacements) up to the parameterization limit,  $\Theta_{\max}(K)$ . Figure 6.4 shows  $\Theta_{\max}(K)$  plotted against the beam angle  $\lambda$ . Furthermore, the individual components of  $K_{\Theta}$ ,  $K_m$  and  $K_f$  were calculated and are plotted in Figure 6.5.

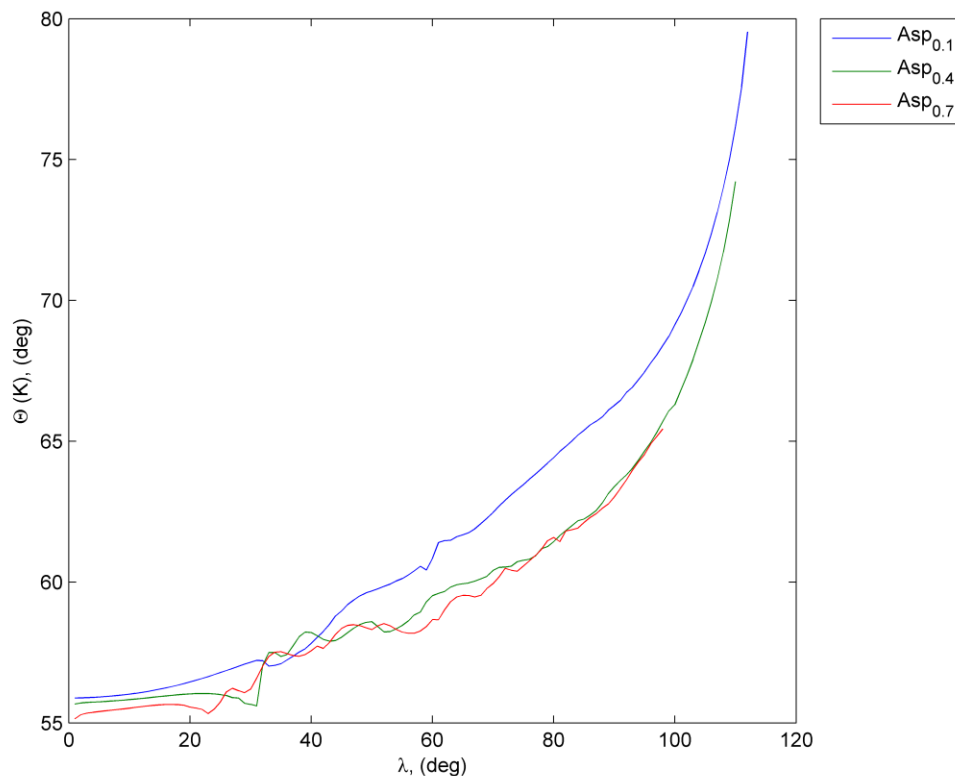


Figure 6.4  $\Theta_{\max}(K)$  versus Lambda

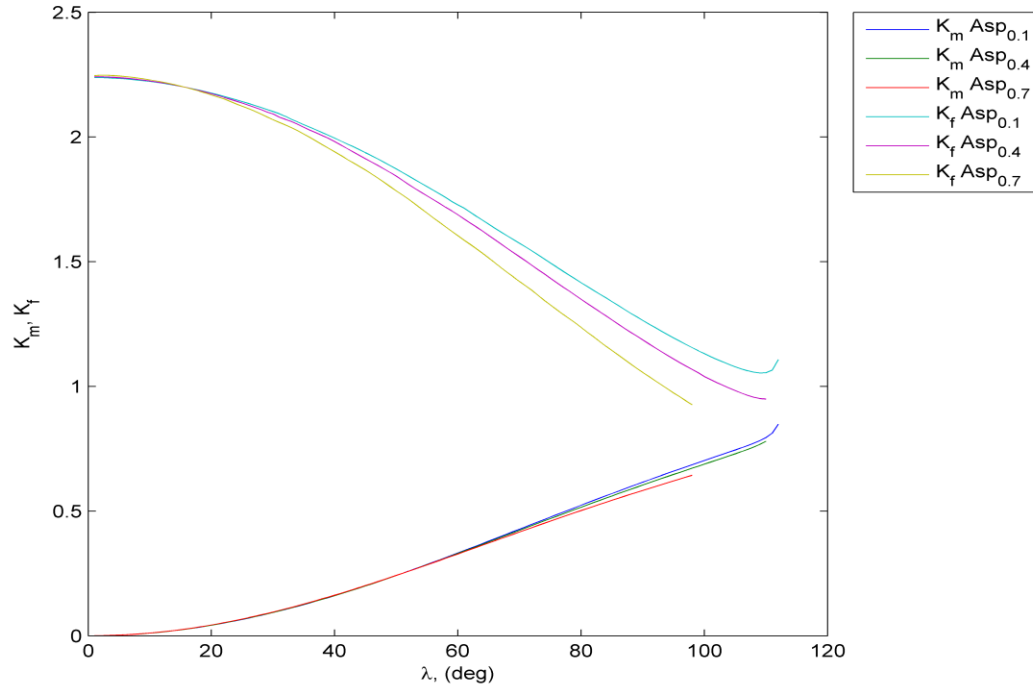


Figure 6.5  $K_m$ ,  $K_f$  versus Lambda

### 6.3 Stress analysis

On the other hand, for a given value of aspect ratio,  $\frac{h}{b}$ , and beam angle,  $\lambda$ , and

characteristic radius factor,  $\gamma$ , one can find a value for the maximum stress at a point P on the beam.

Maximum stress at point P was summed in the following way:

$$\sigma_{\max} = \frac{M_{e1} \cdot c}{I} + \frac{M_{e2} \cdot c}{I} + \frac{M_{e3} \cdot c}{I} + \frac{P_3}{A} \quad (6.1)$$

where  $I$  is the moment of inertia about the neutral axis,  $c$  is the location of the centroid of the beam and  $A$  is the area of the cross-section of the beam, hence:

$$\sigma_{\max} = \frac{c}{I} \begin{bmatrix} (Rf_2(\sin \alpha) + M_{c_3}(\sin \alpha)) \\ R(f_2 \sin \alpha \sin \beta - f_1 \sin \alpha \cos \beta) \\ -(Rf_2(\cos \beta - \cos \alpha) - Rf_1 \sin \beta + M_{c_3}(\cos \alpha)) \end{bmatrix} + \left( \frac{-f_1(\cos \beta \sin \alpha) + f_2(\sin \beta \sin \alpha)}{A} \right)$$

#### 6.4 Conclusion

The kinematics of a compliant curved beam and its rigid body equivalent has been improved. The procedure for analyzing curved compliant beams in a FEA program was improved by writing a batch code. Pseudo-rigid body parameters were calculated from FEA results. These parameters are the characteristic radius factor,  $\gamma$ , the parametric angle coefficient  $c_\theta$ , the parameterization limits  $\Theta_{\max}(\gamma)$ ,  $\Theta_{\max}(K)$  and  $K_\Theta$ . Additionally, a stress analysis was performed on the beam.

## References

- [1] Salamon, B.A., 1989, "Mechanical Advantage Aspects in Compliant Mechanisms Design," in *Advances in Design Automation*, D.A Hoeltzel, ed., 18th ASME Design Automation Conference, DE-Vol44-2, pp. 47-51.
- [2] Sevak, N.M., and McLarman, C.W., 1974, "Optimal Synthesis of Flexible Link Mechanisms with large Static Deflections," ASME Paper 74-DET-83.
- [3] Her, I., 1986, "Methodology for Compliant Mechanisms Design," Ph.D dissertation, Purdue University, West Lafayette, IN.
- [4] Feynman, R.P., "There's Plenty Room at the bottom," *Engineering and Science*, Vol. 23, p. 20, 1960.
- [5] Wilcox, Daniel, 2004, "A fully compliant tensural bistable mechanisms (FTBM) with on-chip thermal actuation." M.S. thesis, Brigham Young University, Provo, UT.
- [6] Howell, L. L. and Midha, A., 1996 "A Loop-Closure theory for the analysis and synthesis of compliant mechanisms" *Journal of mechanical design*, ASME, Vol. 118, No. 1, pp 121-125.
- [7] Howell, L. L., 2001 *Compliant Mechanisms*, 1<sup>st</sup> Ed. Wiley-Interscience, New York, NY.
- [8] Byrd, P.F, and Friedman, M. D., 1954 *Handbook of Elliptic Integrals for Engineers and Physicists*, Springer-Verlag, Berlin.
- [9] Howell, L. L., and Midha, A., 1995, "Parametric Deflection Approximations for End-Loaded, Large Deflection Beams in Compliant Mechanisms," *Journal of Mechanical Design*, ASME, Vol. 117, No.1, pp. 156-165.
- [10] Derderian, J.M., 1996, "The Pseudo-Rigid Body Model Concept and its Application to Micro Compliant Mechanisms," M.S. thesis, Brigham Young University, Provo, UT.
- [11] Mattiasson, K., 1981, "Numerical Results from Large Deflection Beam and Frame Problems Analyzed by Means of Elliptic Integrals," *International Journal for Numerical Methods in Engineering*, Vol. 17, pp 145-153.

- [12] Howell, L. L., and Midha, A., 1995, "Determination of the Degrees of Freedom of Compliant Mechanisms using the Pseudo-Rigid Body Model Concept," Proceedings of the 9th World Congress on the Theory of Machines and Mechanisms, Milano, Italy, Vol. 22, pp. 1537-1541.
- [13] Mohammad H. Dado., 2000, "Variable parametric Pseudo-Rigid-Body Model for Large deflection beams with end loads." International Journal of Non-linear Mechanics, Vol. 36, pp 1123-1133.
- [14] Chao-Chieh Lan and Kok-Meng Lee., "Generalized Shooting Method for Analyzing Compliant Mechanisms," Proceedings of the 2005 IEEE International Conference on Robotics and Automation Barcelona, Spain, April 2005.
- [15] Jinyong Joo, and Sridhar Kota., 2004, "Topological Synthesis of Compliant Mechanisms Using Nonlinear Beam Elements." Mechanics of Structures and Machines. Vol. 32, No. 1, pp. 17–38.
- [16] Chiang, C. H., 1992, *Spherical kinematics in contrast to planar kinematics*, National Taiwan University, Taipei, Taiwan, Mechanical Machine Theory v 27 n 3 May 1992 p 243-250.
- [17] Saurabh Jagirdar, 2006, "Kinematics of Curved Flexible Beam" M.S. thesis, University of South Florida, Tampa, Fl.
- [18] Lusk, C.P., Jagirdar, S., 2007, "Preliminaries for a spherical compliant mechanism: Pseudo-Rigid-Body Model kinematics", ASME paper IDETC/CIE-07
- [19] Spiegel, M. R. and Liu, J., 1999 *Schaum's Outlines: Mathematical Handbook of Formulas and Tables*. McGraw-Hill, Washington, D.C.
- [20] Howell, L. L. and Midha, A., 1994 "The development of force-deflection relationships for compliant mechanisms" *Machine Elements and Machine Dynamics: Proceedings of the 1994 ASME Mechanisms Conference*, DE-Vol. 71. pp. 501-508.
- [21] Paul, B., 1979, *Kinematics and Dynamics of Planar Machinery*, Prentice Hall, Upper Saddle River, NJ.
- [22] Boettama.O. and Roth, B., 1979, *Theoretical Kinematics* Dover, New York.
- [23] Midha, A., and Howell, L.L., 2000, "Limit Positions of Compliant Mechanisms using the Pseudo-rigid-body Model," *Mechanism and Machine Theory*, Vol. 35, No. 1, pp. 99-115.

- [24] Saxena, A. and Kramer, S.N., 1998, "A Simple and Accurate Method for Determining Large Deflections in Compliant Mechanisms Subjected to End Forces and Moments," *Journal of Mechanical Design*, Trans. ASME, Vol. 120, No. 3, pp. 392-400.
- [25] Guerinot A. E., Magleby S. P., and Howell, L.L., 2004 "Preliminary Design Concepts for Compliant Mechanisms Prosthetic Knee Joints", ASME *Mechanisms and Robotics* Conference, Salt Lake City, UT, Sep. 28-Oct. 2, 2004.
- [26] Roach, G.M., and Howell, L. L., 2000, "Compliant Overrunning Clutch with Centrifugal Throw-Out," U.S. patent 6,148,979, Nov 21.
- [27] Crane, N.B., Howell L.L., and Weight, B. L., 2000, "Design and Testing of a Compliant Floating-Opposing Arm (FOA) Centrifugal Clutch," in *Proceedings of 8th International Power Transmission and Gearing Conference, 2000 ASME Design Engineering Technical Conferences DETC2000/PTG-14451*.
- [28] Cannon, J.R., Lusk C.P., and Howell, L.L., 2005 "Compliant Rolling-Contact Element Mechanisms", in *Proceedings of the ASME Mechanisms and Robotics Conference*.
- [29] Jensen, B.D., Howell L.L., and Salmon, L.G., 1999, "Design of Two-Link, In-plane, Bistable Compliant Micro-mechanisms," *Journal of Mechanical Design*, Trans. ASME, Vol. 121, No. 3, pp. 93-96.
- [30] Lai, M.W., Rubin, D., Krempl, E., 1993. *Introduction to Continuum Mechanics 3rd ed.* Butterworth-Heinemann, Woburn, MA.
- [31] Ugural C. A, Fenster K. S, 2003 *Advance Strength and Applied Elasticity*, 4<sup>th</sup> Ed. Prentice Hall, New Jersey, NJ.
- [32] Wolfram, Mathworld, 2006,  
<http://mathworld.wolfram.com/SphericalTriangle.htm>.

## Appendices

## Appendix A: DETC paper

Proceedings of IDETC/CIE  
2007  
ASME 2007 International Design Engineering Technical Conferences and  
Computers and Information in Engineering Conference  
Las Vegas, Nevada, USA, September 4-7, 2007

**DETC2007-34782**

### PRELIMINARIES FOR A SPHERICAL COMPLIANT MECHANISM: PSEUDO-RIGID-BODY MODEL KINEMATICS

**Saurabh Jagirdar**

Department of Mechanical Engineering  
University of South Florida  
4202 East Fowler Avenue ENB 118  
Tampa, FL 33620-5350  
Email: sjagirda@mail.usf.edu

**Craig P. Lusk\***

Department of Mechanical Engineering  
University of South Florida  
4202 East Fowler Avenue ENB 118  
Tampa, FL 33620-5350  
Email: clusk2@eng.usf.edu

#### ABSTRACT

*The kinematic portion of a pseudo-rigid-body model (PRBM) is developed as a generalization from planar to spherical mechanisms. The topology of the spherical compliant segment and its rigid-body equivalent are derived from planar models by analogy. The nomenclature for the spherical PRBM is chosen to facilitate comparison with the planar PRBM. The motion of the compliant segment is calculated using FEA and PRBM parameters are determined. The characteristic radius and parametric angle coefficient are found to decrease as the angle subtended by the beam in-*

*creases. The parameterization limit increases with increasing beam angle. The spherical PRBM is identical to the planar PRBM in the limiting case when beam angles become very small.*

#### 1 INTRODUCTION

This paper describes the kinematic portion of a Pseudo-Rigid-Body Model (PRBM) suitable for the design of a spherical compliant mechanism. As such, the motivation for this work is to expand the scope of previous research on planar compliant mechanisms.

Compliant mechanisms are mechanisms that

---

\*Corresponding Author

## Appendix A (Continued)

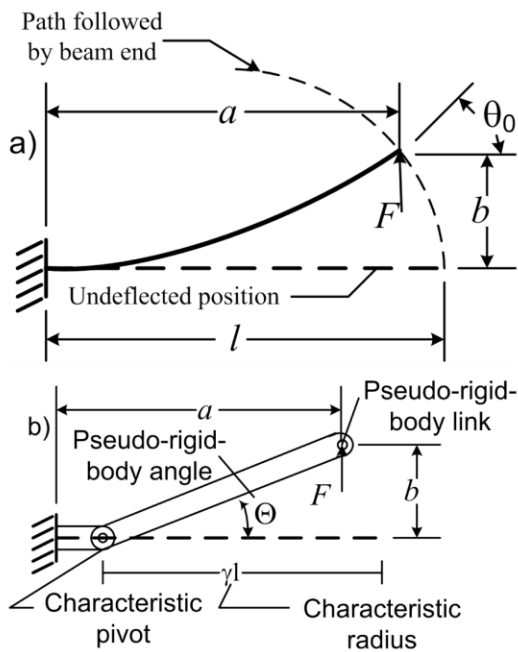


**Figure 1.** A PRBM for a cantilever beam with a vertical end load [4]. Part a) shows the compliant beam and part b) shows the rigid-link equivalent.

for a vertical end-load. These relations are accurate to less than 0.5% error up to the *parameterization limit*,  $\Theta_{max} = 64.3^\circ$ .

In order to determine the spherical analog to the PRBM shown in Fig. 1, we turn to research that has identified correspondences between planar and spherical mechanisms. One example of this correspondence, taken from [29], is shown in Fig. 2 and Fig. 3. Figure 2 shows a planar double-slider mechanism that consists of a straight rigid link connecting sliders traveling on orthogonal lines. The spherical double-slider, shown in Fig. 3 consists of a curved rigid link connecting sliders traveling on orthogonal circles.

The PRBM shown in Fig. 1 may be used to create a partially compliant double slider mechanism as shown in Fig. 4. The partially compliant mechanism differs from the rigid-link mechanism in that the joint between the horizontal slider and the coupler link at  $P$  is changed to a rigid connec-

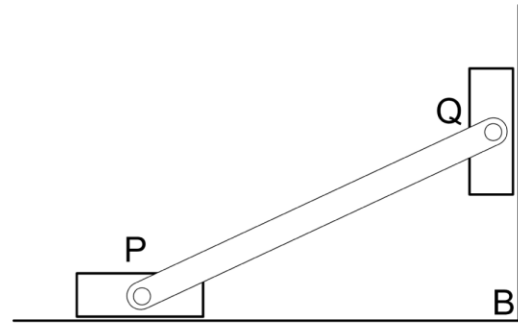


**Figure 2.** Planar mechanism with sliders moving on perpendicular straight lines

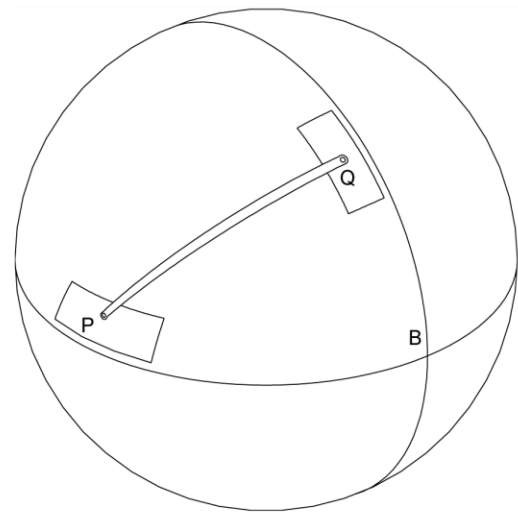


**Figure 3.** Spherical mechanism with sliders moving on perpendicular circular arcs

tion and the coupler link itself is changed to a compliant link.

The compliant analog of the spherical double slider can then be deduced by applying the same procedure. The joint between the horizontal slider and the curved coupler link is changed to a rigid connection and the coupler link is changed to a compliant link. The resulting partially-compliant spherical double-slider mechanism is shown in Fig. 5. The comparison between Fig. 3 and Fig. 5 suggests the spherical PRBM described in the next

## Appendix A (Continued)

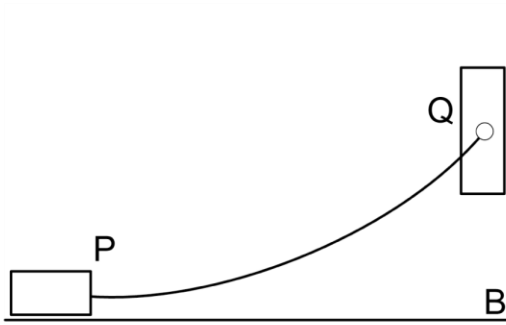


**Figure 4.** *Compliant planar mechanism with sliders moving on perpendicular straight lines*

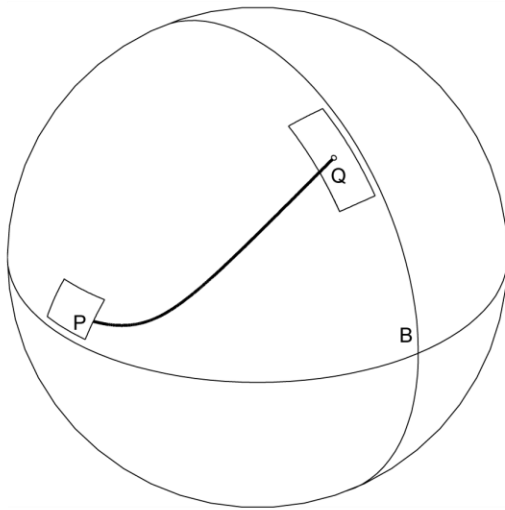


**Figure 5.** *Spherical compliant mechanism with sliders moving on perpendicular circles*

section.

This analogy-based derivation of a spherical compliant mechanism can be amplified by the following consideration. Mechanisms whose joint axes are parallel to each other are known as planar mechanisms [28]. In planar compliant mechanisms, this characteristic is achieved by designing straight flexures that, at each point along their length, are most flexible about parallel lines and considerably more rigid in other directions. On the other hand, mechanisms whose joint axes intersect

at a point are spherical mechanisms [28]. In spherical compliant mechanisms, this characteristic can be achieved with curved flexures that, at each point along the arc, are most flexible about lines that intersect at a common point. This suggests that the neutral axis of the undeflected beam should be circular and that the beams should be wider in the radial direction and thin in direction perpendicular to both the neutral axis and the radial direction. This insures that the bending stiffness of the beam is smallest about radial lines. Furthermore, the thinner and wider the beam is, the less tendency it has to twist.

## 2 SPHERICAL PRBM TOPOLOGY AND NOMENCLATURE

There is a correspondence principle between spherical mechanisms and planar mechanisms: Spherical mechanisms whose arc lengths are much smaller than the radius of the sphere closely approximate planar mechanisms. In fact, spherical kinematics is identical to the planar kinematics in the limiting case when the radius of the sphere is infinitely larger than the links. We emphasize this correspondence principle in deriving the spherical PRBM from the planar PRBM by using the Greek letter to denote an arc that corresponds to a line denoted with a Roman letter. For example, the spherical angle,  $\beta$ , corresponds to the planar dimension,  $b$ . Similarly, the angles  $\alpha$  and  $\lambda$  correspond to the dimensions  $a$  and  $l$ , respectively.

The correspondence principle means that it is possible to give the same names to equivalent dimensionless parameters. For example, the pseudo-rigid-body angle,  $\Theta$ , and the beam inclination angle,  $\theta_0$ , appear in both the planar and spherical models as do ratios, e.g. the characteristic radius factor,  $\gamma$ , and the parametric angle coefficient,  $c_\theta$ .

### 2.1 The Displacement of a Compliant Curved Beam

The displacement of the compliant curved cantilever,  $PQ$ , is described by using a series of coordinate frames, as shown in Fig. 6. The fixed end of the curved cantilever beam is denoted as  $P$  and

## Appendix A (Continued)

free end of the beam as  $Q$ . Let  $S$  be a sphere whose center is defined by  $O$  frame. The frames  $A$ ,  $B$ ,  $C$  and  $D$  are on the surface of the sphere. The position and orientation of the coordinate frames are related as follows:

- The  $O$  frame is attached to the center of the sphere. The  $o_1$  axis passes through the undeflected beam end  $Q$ . The  $o_2$  axis is normal to the plane containing the undeflected beam. The  $o_3$  axis completes the right-handed orthogonal triad and is parallel with the neutral axis of the undeflected beam end at  $Q$ .
- The  $A$  frame has the same orientation as the  $O$  frame and is located at the end of the undeflected beam.
- The  $B$  frame locates the deflected position of the beam end  $Q$  in the  $a_1 - a_3$  plane (analogous to the translation in the  $x$ -direction in the planar model).
- The  $C$  frame describes movement of beam end  $Q$  in the  $b_2 - b_1$  plane rotating about point  $O$  (analogous to the translation in the  $y$ -direction in the planar model).
- The  $D$  frame is at the same position as the  $C$  frame and tracks the rotation of the beam end about the radial axis through the beam end (analogous to the rotation of the beam end about the  $z$ -axis in the planar model).

The frames are described by the matrices  $A$ ,  $B$ ,  $C$  and  $D$ , where the columns of the matrix are the basis vectors. The transformations relating the frames are given by:

$$A = [\{\hat{a}_1\}, \{\hat{a}_2\}, \{\hat{a}_3\}] \quad (4)$$

$$= \begin{bmatrix} 1 & 0 & 0 \\ 0 & 1 & 0 \\ 0 & 0 & 1 \end{bmatrix} \quad (5)$$

$$B = [\{\hat{b}_1\}, \{\hat{b}_2\}, \{\hat{b}_3\}] \quad (6)$$

$$= \begin{bmatrix} \cos(\phi) & 0 & -\sin(\phi) \\ 0 & 1 & 0 \\ \sin(\phi) & 0 & \cos(\phi) \end{bmatrix} A \quad (7)$$

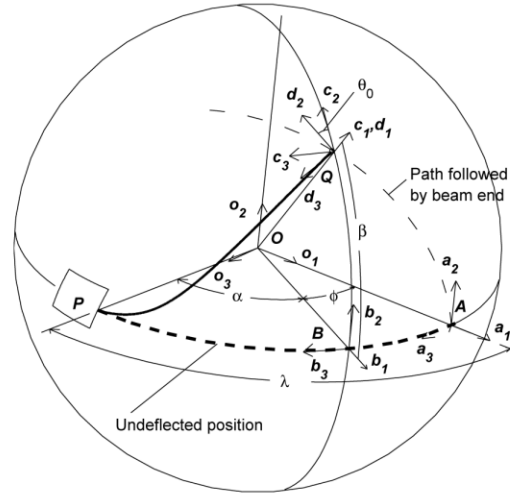


**Figure 6.** Reference frames describing the motion of the end of a compliant curved cantilever

$$= R(\hat{a}_2, -\phi)A \quad (8)$$

$$C = [\{\hat{c}_1\}, \{\hat{c}_2\}, \{\hat{c}_3\}] \quad (9)$$

$$= \begin{bmatrix} \cos(\beta) & -\sin(\beta) & 0 \\ \sin(\beta) & \cos(\beta) & 0 \\ 0 & 0 & 1 \end{bmatrix} B \quad (10)$$

$$= R(\hat{b}_3, \beta)B \quad (11)$$

$$D = [\{\hat{d}_1\}, \{\hat{d}_2\}, \{\hat{d}_3\}] \quad (12)$$

$$= \begin{bmatrix} 1 & 0 & 0 \\ 0 & \cos(\theta_0) & -\sin(\theta_0) \\ 0 & \sin(\theta_0) & \cos(\theta_0) \end{bmatrix} C \quad (13)$$

$$= R(\hat{c}_1, \theta_0)C \quad (14)$$

Thus, the deflection of the curved cantilever beam is described by the kinematic parameters  $\phi = \lambda - \alpha$ ,  $\beta$  and  $\theta_0$ , which are the spherical equivalents to the dimensions  $l - a$ ,  $b$  and  $\theta_0$  shown in Fig. 1.

These frames can also be used, with minimal modification, to describe the spherical double-slider model. In this interpretation, the definition

## Appendix A (Continued)

of the  $O$  frame is unchanged. The  $B$  frame has the same orientation as the  $O$  frame, and the  $A$  rotates around the sphere to track the rotation of the slider at  $P$ , i.e. the  $A$  frame is always an angle  $\lambda$  away from the location of point  $P$ . Thus, in the double slider,  $B$  is the identity matrix and  $A = R(b_2, \phi)B$ ,  $C = R(b_3, \beta)B$ , and  $D = R(c_1, \theta_0)C$ . The only difference between the cantilever model and the double-slider model is that in the cantilever model, the  $A$  frame has the same orientation as the  $O$  frame; while in the double-slider model, the  $B$  frame has the same orientation as the  $O$  frame. The relative positions and orientations of the  $A$ ,  $B$ ,  $C$ , and  $D$  frames are identical. Thus, we are free to solve the problem using the most convenient model, which happens to be the double-slider, and interpret the results in terms of either the double-slider model or the cantilever model.

### 2.2 Spherical Pseudo-Rigid-Body Model Kinematics

In both planar and spherical PRBMs,  $\Theta$  is defined as the pseudo-rigid-body angle, i.e. the rotation of the characteristic-pivot (pseudo-pivot) and the characteristic radius factor,  $\gamma$ , is defined as the length from the beam end to the pseudo-pivot divided by the length of the beam.

The pseudo-rigid-body model of the compliant beam shown in Fig. 6 is shown in Fig. 7. The compliant beam's neutral axis subtends an arc,  $\lambda$ , and its PRBM consists of two rigid links, which subtend circular arcs of  $\gamma\lambda$  and  $(1 - \gamma)\lambda$ , and are joined by a revolute joint. The axis of the revolute joint passes through the center of the sphere.

The relationships for  $\alpha$  and  $\beta$  in terms of  $\gamma$  and  $\Theta$  are obtained using Napier's rules for right spherical triangles [30] on the triangle shown in Fig. 7 with sides  $\gamma\lambda$ ,  $\gamma\lambda - \phi$ , and  $\beta$ . We find  $\phi$  as a function of  $\gamma\lambda$  and  $\Theta$  as

$$\phi = \gamma\lambda - \tan^{-1}(\tan \gamma\lambda \cos \Theta) \quad (15)$$

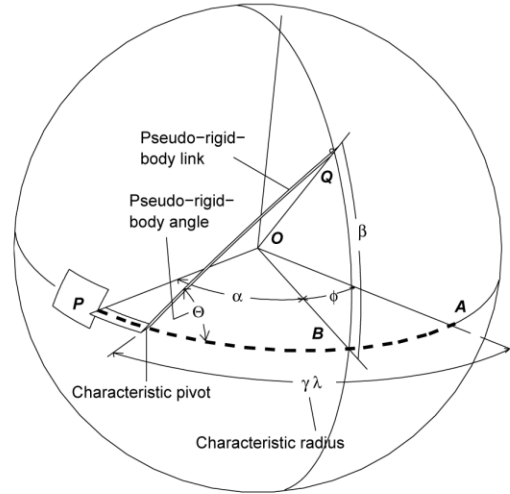


Figure 7. The pseudo-rigid-body model of the compliant curved beam shown in Figure 6

The horizontal angle,  $\alpha$ , is

$$\alpha = \tan^{-1}(\tan \gamma\lambda \cos \Theta) \quad (16)$$

The vertical angle,  $\beta$ , is

$$\beta = \sin^{-1}(\sin \gamma\lambda \sin \Theta) \quad (17)$$

### 3 FINITE ELEMENT MODEL

To compute the deflection of the curved beam undergoing spherical motion, the beam is modeled in a commercial FEA software package (ANSYS 10). Three-dimensional beam elements with 6 degrees-of-freedom (BEAM4) were used. Because large deflection analysis was required, the iterative nonlinear solver was used. The loading conditions proved easiest to apply using the double-slider model.

The FEA model consisted of a compliant circular segment  $PQ$  and a straight rigid segment  $OP$ . The modulus of elasticity of the compliant circular segment was taken as one thousandth that of the rigid segment. The purpose of the straight rigid segment was to insure that the end  $P$  of the compliant segment moved in pure rotation about  $O$  in the

## Appendix A (Continued)

$o_1 - o_3$  plane. This was accomplished by applying boundary conditions to the rigid segment  $OP$  which prevent all translation and permitted rotation only about the  $o_2$  axis. The motion of point  $Q$  was determined by the magnitude of the input parameter  $\beta$ . The displacement in the  $o_1$  direction was  $|OQ|(\cos\beta - 1)$ , and the displacement in the  $o_2$  direction was  $|OQ|\sin\beta$ . No translation was permitted in the  $o_3$  direction. Point  $Q$  was also constrained to rotate an amount  $\beta$  about the  $o_3$  axis and was permitted to rotate freely about the  $o_1$  and  $o_2$  axes.

Thus, the input parameter is the angle  $\beta$  which determines both the rotation of the beam end  $Q$  and its deflection. One output obtained is the rotation angle,  $\phi = \lambda - \alpha$ , of the beam end  $P$  as it moves along a circular arc in the  $b_1$ - $b_3$  plane. The other output is the rotation,  $\theta_0$ , of the neutral axis of the beam at  $Q$  about the radial axis.

The simulation was repeated varying: a) the initial beam angle  $\lambda$  b) the aspect ratio of the curved flexible beam, or its width divided by its thickness,  $b/h$ . Simulations were run for beam angles ranging from 4 degrees to 112 degrees in increments of 2 degrees and aspect ratios of 0.1, 0.4 and 0.7. The values of the input displacement,  $\beta$  were applied in 200 even increments ranging from 0 degrees up to the beam angle,  $\lambda$ .

The parametric angle coefficient,  $c_\theta$ , the characteristic radius factor,  $\gamma$ , and the parameterization limit,  $\Theta_{max}$ , are obtained from the results of the FEA model using the procedure described in the next section.

### 4 PSEUDO-RIGID-BODY MODEL PARAMETERS

We follow Howell's method [4] for determining PRBM parameters. An optimal value for the characteristic radius factor,  $\gamma$ , may be found given a maximum acceptable percentage error in deflection. We found the value of  $\gamma$  that would allow the maximum pseudo-rigid-body angle,  $\Theta$ , while keeping the error in the position of the beam end less than 0.5%.

Napier's rules can be used to express the de-

pendence of the pseudo-rigid-body angle,  $\Theta$ , on  $\gamma$  for the spherical PRBM.

$$\sin\beta = \sin\Theta \sin\gamma\lambda \quad (18)$$

$$\cos\Theta = \tan(\gamma\lambda - \phi) \cot\gamma\lambda \quad (19)$$

Therefore,

$$\Theta = \tan^{-1} \left[ \frac{\sin\beta}{\tan(\gamma\lambda - \phi) \cos\gamma\lambda} \right] \quad (20)$$

which is subject to the parametric constraint

$$g(\Theta) = error/\varepsilon_e \leq (error/\varepsilon_e)_{max} \quad (21)$$

where  $error/\varepsilon_e$  is the relative deflection error, and  $\varepsilon_e$  is defined as the vector difference of the deflected position of point  $Q$  and its original undeflected position.

The deflection obtained using FEA,  $\varepsilon_e$ , is shown in Fig. 8 and can be calculated from the beam motion parameters,  $\beta$  and  $\phi$  as:

$$\varepsilon_e = R(b_3, \beta)R(a_2, -\phi)a_1 - a_1 \quad (22)$$

$$= \begin{bmatrix} \cos\beta \cos\phi - 1 \\ \sin\beta \\ \cos\beta \sin\phi \end{bmatrix} \quad (23)$$

The PRBM deflection estimate,  $\varepsilon_a$ , is given by the vector difference of the deflected location of point  $Q$  calculated using the PRBM and its undeflected coordinates, or  $\vec{\varepsilon}_a = \vec{Q} - a_1$ .

From Fig. 7, the position of point  $Q$  according to the PRBM is  $\vec{Q} = R\vec{a}_1$ , where  $R$  is the rotation operator that acts on the vector  $a_1$  and rotates it about the pseudo pivot,  $\vec{m}$ , through an angle  $\Theta$ . The action of the operator  $R$  on  $\vec{a}_1$  is given [32] by:

## Appendix A (Continued)

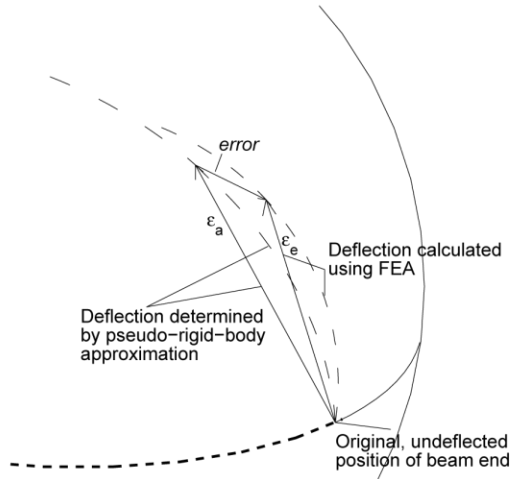


**Figure 8.** Schematic showing the displacement of the compliant beam,  $\epsilon_e$ , the estimate of the displacement using the PRBM,  $\epsilon_a$ , and the error. Adapted from [4]

$$\begin{aligned}\vec{Q} &= R\vec{a}_1 \\ &= (1 - \cos\Theta)(\vec{m} \cdot \vec{a}_1)\vec{m} \\ &\quad + \cos\Theta\vec{a}_1 + \sin\Theta(\vec{m} \times \vec{a}_1)\end{aligned}\quad (24)$$

where  $\vec{m} = \begin{bmatrix} \cos\gamma\lambda \\ 0 \\ \sin\gamma\lambda \end{bmatrix}$  and  $\vec{a}_1 = \begin{bmatrix} 1 \\ 0 \\ 0 \end{bmatrix}$ ,  
which reduces to

$$\vec{Q} = R\vec{a}_1 = \begin{bmatrix} \cos^2\gamma\lambda(1 - \cos\Theta) + \cos\Theta \\ \sin\gamma\lambda\sin\Theta \\ \cos\gamma\lambda\sin\gamma\lambda(1 - \cos\Theta) \end{bmatrix}\quad (25)$$

Therefore,

$$\epsilon_a = \begin{bmatrix} \cos^2\gamma\lambda(1 - \cos\Theta) + \cos\Theta - 1 \\ \sin\gamma\lambda\sin\Theta \\ \cos\gamma\lambda\sin\gamma\lambda(1 - \cos\Theta) \end{bmatrix}\quad (26)$$

The *error* is defined as magnitude of the vector difference between the final positions of the curved

flexible segment found using FEA and the final position found using the pseudo-rigid body model with a particular value of  $\gamma$ .

The *error* in the deflection is calculated as

$$\begin{aligned}error &= |\vec{\epsilon}_e - \vec{\epsilon}_a| \\ &= \sqrt{(\epsilon_{ex} - \epsilon_{ax})^2 + (\epsilon_{ey} - \epsilon_{ay})^2 + (\epsilon_{ez} - \epsilon_{az})^2}\end{aligned}\quad (27)$$

The relative error,  $error/\epsilon_e$  is defined as

$$error/\epsilon_e = \frac{|\vec{\epsilon}_e - \vec{\epsilon}_a|}{|\vec{\epsilon}_e|}\quad (28)$$

The value of the pseudo-rigid-body angle,  $\Theta$  at the point at which the relative error equals or exceeds an acceptable amount is the parameterization limit  $\Theta_{max}$ .

## 5 RESULTS AND DISCUSSION

For a given value of aspect ratio,  $h/b$ , and beam angle,  $\lambda$ , one can find a value of characteristic radius factor,  $\gamma$ , and parametric angle coefficient,  $c_\Theta$ , that best approximates the motion (position and orientation of beam at various input displacements) up to the parameterization limit,  $\Theta_{max}$ .

The characteristic radius factor,  $\gamma$ , the parametric angle coefficient,  $c_\Theta$ , and the parameterization limit,  $\Theta_{max}$ , obtained for aspect ratios of  $h/b = 0.1, 0.4, 0.7$  are plotted in Fig. 9 and Fig. 10 and in Fig. 11, respectively.

A regression line for the characteristic radius factor,  $\gamma$ , as a function of the arc subtended by the beam for values  $16^\circ \leq \lambda \leq 112^\circ$  is computed for aspect ratios  $h/b = 0.1, 0.4$  and  $0.7$ . The variance accounted for by the fit is given by an  $R^2$  value and a two-sided 95% confidence interval is given for each coefficient.

For aspect ratio  $h/b = 0.1$ :  $R^2 = 0.9998$   
 $\gamma = (0.8523 \pm 0.0008) + (-6.2 \pm 4.8) \times 10^{-5}\lambda + (-2.3 \pm 0.8) \times 10^{-6}\lambda^2 + (-2.5 \pm 0.4) \times 10^{-8}\lambda^3$ .

For aspect ratio  $h/b = 0.4$ :  $R^2 = 0.9999$

## Appendix A (Continued)

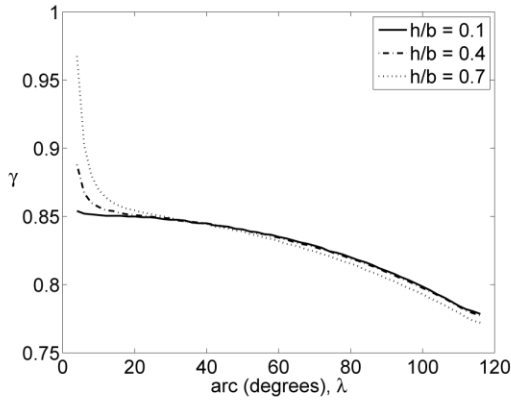


**Figure 9.** Characteristic radius factor,  $\gamma$ , versus beam angle,  $\lambda$ . The line for aspect ratio  $h/b = 0.1$  is a solid line, aspect ratio  $h/b = 0.4$  is shown with long dashes, and aspect ratio  $h/b = 0.7$  is shown with short dashes.

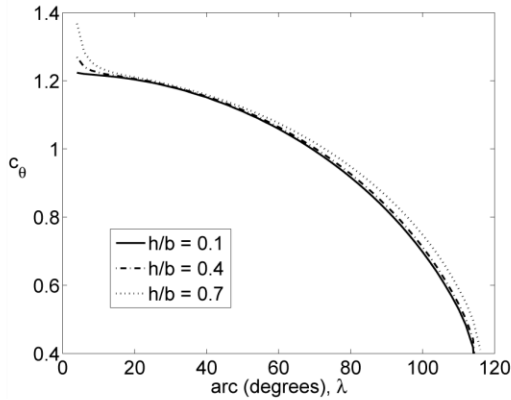


**Figure 10.** Parametric angle coefficient,  $c_\theta$ , versus beam angle,  $\lambda$ . The line for aspect ratio  $h/b = 0.1$  is a solid line, aspect ratio  $h/b = 0.4$  is shown with long dashes, and aspect ratio  $h/b = 0.7$  is shown with short dashes.

$$\gamma = (0.8553 \pm 0.0007) + (-1.6 \pm 0.4) \times 10^{-4}\lambda + (-1.3 \pm 0.7) \times 10^{-6}\lambda^2 + (-2.7 \pm 0.4) \times 10^{-8}\lambda^3.$$

$$\text{For aspect ratio } h/b = 0.7: R^2 = 0.9997$$

$$\gamma = (0.8644 \pm 0.0012) + (-5.3 \pm 0.7) \times 10^{-4}\lambda + (2.1 \pm 1.2) \times 10^{-6}\lambda^2 + (-4.0 \pm 0.6) \times$$

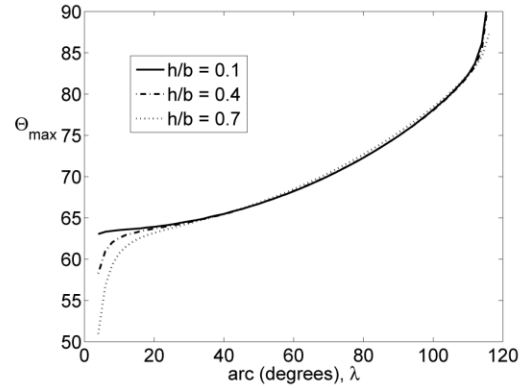


**Figure 11.** Parameterization limit,  $\Theta_{max}$ , versus beam angle,  $\lambda$ . The line for aspect ratio  $h/b = 0.1$  is a solid line, aspect ratio  $h/b = 0.4$  is shown with long dashes, and aspect ratio  $h/b = 0.7$  is shown with short dashes.

$$10^{-6}\lambda^3.$$

Similarly, a regression line for the parametric angle coefficient,  $c_\theta$ , as a function of the arc subtended by the beam for values  $16^\circ \leq \lambda \leq 112^\circ$ .

$$\text{For aspect ratio } h/b = 0.1: R^2 = 0.9995$$

$$c_\theta = (1.265 \pm 0.015) + (-3.5 \pm 0.9) \times 10^{-3}\lambda + (3.7 \pm 1.5) \times 10^{-5}\lambda^2 + (-6.0 \pm 0.7) \times 10^{-7}\lambda^3.$$

$$\text{For aspect ratio } h/b = 0.4: R^2 = 0.9995$$

$$c_\theta = (1.271 \pm 0.014) + (-3.7 \pm 0.8) \times 10^{-3}\lambda + (4.3 \pm 1.4) \times 10^{-5}\lambda^2 + (-6.2 \pm 0.7) \times 10^{-5}\lambda^3.$$

$$\text{For aspect ratio } h/b = 0.7: R^2 = 0.9995$$

$$c_\theta = (1.282 \pm 0.014) + (-4.2 \pm 0.8) \times 10^{-3}\lambda + (5.2 \pm 1.3) \times 10^{-5}\lambda^2 + (-6.4 \pm 0.7) \times 10^{-7}\lambda^3.$$

### 5.1 Small Angle Validation

Spherical mechanisms whose arc lengths are much smaller than the radius of the sphere closely approximate planar mechanisms. In fact, spherical kinematics is identical to the planar kinematics in the limiting case when the radius of the sphere is infinitely larger than the links. Thus, for small values of beam angle, e.g.  $\lambda = 4^\circ$ , the calculated pa-

## Appendix A (Continued)

rameters for characteristic radius factor, parametric angle coefficient and parameterization limit should and do approach the values reported in the literature,  $\gamma = 0.85$ ,  $c_\theta = 1.24$ , and  $\Theta_{max} = 64.3^\circ$  for the planar case [4]. It is interesting to note that this relationship holds best when the aspect ratio,  $h/b$ , is smallest. We note that the values for characteristic radius factor and parametric angle coefficient decrease as the angle subtended by the beam increases. On the other hand, the parameterization limit increases with increasing beam angle.

### 6 CONCLUSIONS

The kinematic portion of a Pseudo-Rigid-Body Model (PRBM) for spherical mechanisms has been developed. The kinematics of a compliant curved beam and its rigid-body equivalent were described. The procedure for analyzing the curved compliant beams in a FEA program was developed. Pseudo-rigid body parameters were calculated from FEA results. These parameters are the characteristic radius factor,  $\gamma$ , the parametric angle coefficient,  $c_\theta$  and the parameterization limit  $\Theta_{max}$ . These values approach the values found in the planar case for long thin beams with small arc-lengths. These results permit the kinematics of a circular cantilever or a compliant spherical double-slider mechanism to be modeled as a rigid body under appropriate displacement loading conditions.

### 7 REFERENCES

- [1] Salamon, B.A., 1989, "Mechanical Advantage Aspects in Compliant Mechanisms Design," in *Advances in Design Automation, D.A Hoeltzel, ed., 18th ASME Design Automation Conference*, pp. 47-51.
- [2] Her, I., and Midha, A., 1987, "A Compliance Number Concept for Compliant Mechanisms, and Type Synthesis." *Journal of Mechanisms, Transmissions, and Automation in Design, Trans. ASME*, Vol. 109, No. 3, pp. 348-355.
- [3] Sevak, N.M., and McLarman, C.W., 1974, "Optimal Synthesis of Flexible Link Mechanisms with large Static Deflections," *ASME Paper 74-DET-83*.
- [4] Howell L. L., 2001, *Compliant Mechanisms*, John Wiley and Sons, Inc, NY.
- [5] Midha, A., Her, I., and Salamon, B.A., 1992, "A Methodology for Compliant Mechanisms Design, Part I: Introduction and Large-Deflection Analysis," in *Advances in Design Automation, D.A Hoeltzel, ed., 18th ASME Design Automation Conference*, pp. 29-38.
- [6] Midha, A., and Howell, L.L., 2000, "Limit Positions of Compliant Mechanism using the Pseudo-rigid body Model," *Mechanism and Machine Theory*, Vol. 35, No. 1, pp. 99-115.
- [7] Howell, L. L., and Midha, A., 1994, "The development of Force Deflection Relationships," *Machine elements and Machine Dynamics: Proceedings of the 1994 ASME Mechanisms conference*, Vol. 71, pp. 501-508.
- [8] Howell, L. L., and Midha, A., 1995, "Parametric Deflection Approximations for End-Loaded, Large Deflection Beams in Compliant Mechanisms," *Journal of Mechanical Design*, Vol. 117, No.1, pp. 156-165.
- [9] Howell, L. L., and Midha, A., 1995, "Determination of the Degrees of Freedom of Compliant Mechanisms using the Pseudo-Rigid Body Model Concept," in *Proceedings of the 9th World Congress on the Theory of Machines and Mechanisms, Milano, Italy*, Vol. 22, pp. 1537-1541.
- [10] Saxena, A. and Kramer, S.N., 1998, "A Simple and Accurate Method for Determining Large Deflections in Compliant Mechanisms Subjected to End Forces and Moments," *Journal of Mechanical Design*, Trans. ASME, Vol. 120, No.3, pp. 392-400.
- [11] Dado M. H., 2001, "Variable Parametric Pseudo-Rigid Body Model for Large Deflection Beams with End Loads," *International Journal of Non-linear Mechanics*, Volume 36, Issue 7, October 2001, Pages 1123-1133.
- [12] Baker, M.S., Lyon, S.M., and Howell L.L., 2000, "A Linear Displacement Bistable Micromechanism," in *Proceedings of the 26th Biennial Mechanisms and Robotics Conference*,

## Appendix A (Continued)

- 2000 ASME Design Engineering Technical Conferences, DETC2000/MECH-14119.
- [13] N.B. Hubbard, L.L. Howell, 2005 "Design and Characterization of a Dual-stage, Thermally Actuated Nanopositioner", *Journal of Micromechanics and Microengineering*, Vol. 15, pp. 1482-1493.
- [14] Ananthasuresh, G.K., Kota, S., and Gianchandani, Y., 1994, "A Methodical Approach to the Design of Compliant Micro-mechanisms," *Solid-State Sensor and Actuator Workshop, Hilton Head Island, SC*, pp. 189-192.
- [15] Ananthasuresh, G. K., and Kota, S., 1995, "Designing of Compliant Mechanisms," *Mechanical Engineering*, Vol. 117, No.11, pp. 93-96.
- [16] Jensen, B.D., Howell L.L., Gunyan, D.B., and Salmon, L.G., 1997, "The Design and Analysis of Compliant MEMS Using the Pseudo-Rigid-Body Model," *Micromechanical Systems (MEMS), at the 1997 ASME International Mechanical Engineering Congress and Exposition*, Vol. 62, pp. 119-126.
- [17] Salmon, L.G., Gunyan, D.B., Derderian, J.M., Opdahl, P.G., and Howell L.L., 1996, "Use of the Pseudo-Rigid Body Model to Simplify the Description of Compliant Micromechanisms," *1996 IEEE Solid-State and Actuator Workshop, Hilton Head Island, SC*, pp. 136-139.
- [18] Brocket, W. R. and Stokes, A., 1991 "On the Synthesis of Compliant Mechanisms," in *Proceedings of the 1991 IEEE International Conference on Robotics and Automation*, Apr 9-11 1991, Sacramento, CA, Vol. 3, pp. 2168-2173.
- [19] Saggere, L. and Kota, S., 1997 "Synthesis of Distributed Compliant Mechanisms for Adaptive Structure application: An Elasto-Kinematic Approach" in *Proceedings of the ASME Design Engineering Technical Conferences*, September 14-17, Sacramento, California.
- [20] Guerinet A. E., Magleby S. P., and Howell, L. L., 2004 "Preliminary Design Concepts for Compliant Mechanism Prosthetic Knee Joints", *ASME Mechanisms and Robotics Conference*, Salt Lake City, UT, Sep. 28-Oct. 2, 2004.
- [21] Roach, G.M., and Howell, L. L., 2000, "Compliant Overrunning Clutch with Centrifugal Throw-Out," U.S. patent 6,148,979, Nov 21.
- [22] Crane, N.B., Howell L.L., and Weight, B. L., 2000, "Design and Testing of a Compliant Floating-Opposing Arm (FOA) Centrifugal Clutch," in *Proceedings of 8th International Power Transmission and Gearing Conference, 2000 ASME Design Engineering Technical Conferences DETC2000/PTG-14451*.
- [23] Cannon, J.R., Lusk C.P., and Howell, L.L., 2005 "Compliant Rolling-Contact Element Mechanisms", in *Proceedings of the ASME Mechanisms and Robotics Conference*.
- [24] Millar, A. J., Howell L. L., and Leonard, J. N., 1996 "Design and Evaluation of Compliant Constant Force Mechanisms," in *Proceedings of the 1996 ASME DETC and Computers in Engineering Conference 96-DETC/ MECH-1209*.
- [25] Derderian, J.M., 1996, "The Pseudo-Rigid Body Model Concept and its Application to Micro Compliant Mechanisms," M.S. thesis, Brigham Young University, Provo, UT.
- [26] Jensen, B.D., Howell L.L., and Salmon, L.G., 1999, "Design of Two-Link, In-plane, Bistable Compliant Micro-mechanisms," *Journal of Mechanical Design*, Trans. ASME, Vol. 121, No. 3, pp. 93-96.
- [27] Lusk, C.P., and Howell, L.L., 2005, "Components, Building Blocks, and Demonstrations of Spherical Mechanisms for Microelectromechanical Systems," in *Proceedings of the 2005 ASME Mechanisms and Robotics Conference*, DETC2005-84672.
- [28] McCarthy, J., 2000 *Geometric Design of Linkages* Springer, NY.
- [29] Chiang, C. H., 1988, *Kinematics of Spherical Mechanisms*, Cambridge, New York, NY.
- [30] Spiegel, M. R. and Liu, J., 1999 *Schaum's Outlines: Mathematical Handbook Of Formulas And Tables*. McGraw-Hill, Washington, D.C.

## Appendix A (Continued)

- [31] Henderson, D. W., 1998 *Differential Geometry*, Prentice Hall Upper Saddle River, NJ.
- [32] Lai, M.W., Rubin, D., Krempl, E., 1993. *Introduction to Continuum Mechanics 3rd ed.* Butterworth-Heinemann, Woburn, MA.

## Appendix B: ANSYS batch code

```
!*****
/CONFIG,NRES,10000
!/CWD,'C:\Documents and Settings\aleon2\Desktop\Work'

!*****

!*****
!***** Set Up Model Variables *****
!*****

!*DO,asp, .4,.7,.3
asp =.1
aspect = 10*asp
*DO,arclength,1,126,1      ! this is really the angle subtended by arc
!arclength=40

/title,3D Beam Non-linear Deflection
/PREP7
LCLEAR, ALL
LDELETE, ALL
KDELETE, ALL

R=100
PI=acos(-1.)
T_arclength = R*arclength*PI/180 ! this is the true arc length of the beam
h1=.1*T_arclength      ! make the height and width small in comparison to the
length of the beam
b1=h1

b2=.1*T_arclength
h2=asp*b2

!***** Area properties *****
A1 = h1*b1
Iy1= 1/12*b1*h1*h1*h1      ! this is the I value for the bending direction-use it to
normalize the forces
Iz1= 1/12*h1*b1*b1*b1
E1= 3000000
!*****
```

## Appendix B (Continued)

$$A2= h2*b2$$

$$Iz2= 1/12*h2*b2*b2*b2$$

$$Iy2= 1/12*b2*h2*h2*h2$$

$$E2= 300$$

!\*\*\*\*\* Declare an element type: Beam 4 (3D Elastic) \*\*\*\*\*

ET,1,BEAM4

KEYOPT,1,2,1

KEYOPT,1,6,1

!\*\*\*\*\* Set Real Constants and Material Properties \*\*\*\*\*

R,1,A1,Iy1,Iz1,h1,b1, , !\*\*\*\*\*Check on the assumptions being made \*\*\*\*\*

R,2,A2,Iy2,Iz2,h2,b2, ,

MPTEMP,1,0

MPDATA,EX,1,,E1

MPDATA,PRXY,1,,0.35 ! Material properties for material 1 and 2

MPTEMP,1,0

MPDATA,EX,2,,E2

MPDATA,PRXY,2,,0.35

!\*\*\*\*\*

xcoor=R\*cos(arclength\*PI/180)

zcoor=R\*sin(arclength\*PI/180)

!\*\*\*\*\* Create Keypoints 1 throug 7: K(Point #, X-Coord, Y-Coord, Z-Coord)

\*\*\*\*\*

K,1,0,0,0,

K,2,xcoor,0,zcoor,

K,3,R,0,0,

K,4,1.050\*R,0,0,

K,5,R,.050\*R,0,

K,6,R,0,-.050\*R,

K,7,.950\*R,0,0

!\*\*\*\*\* Create Beam using Lines and an Arc and divide into segments \*\*\*\*\*

LSTR, 1, 2

LSTR, 3, 4

! Draws lines connecting keypoints 1 through 7

LSTR, 3, 5

LSTR, 3, 6

LSTR, 3, 7

## Appendix B (Continued)

LESIZE,ALL,,2                   ! Specifies the divisions and spacing ratio on unmeshed lines, 2 divisions on lines 1 through 7 except 6  
LARC,2,3,1,R,                   ! Defines a circular arc  
LESIZE,6,,32                   ! Specifies the divisions and spacing ratio on unmeshed lines, 32 divisions on line 6

!\*\*\*\*\* MESH \*\*\*\*\*

real,1                   ! Use real constant set 1  
type,1                   ! Use element type 1  
mat,1                   ! use material property set 1  
LMESH,1,5               ! mesh lines 1-5

real,2                   ! Use real constant set 2  
type,1                   ! Use element type 1  
mat,2                   ! use material property set 2  
LMESH,6               ! mesh line 6

!\*\*\*\*\* Get Node Numbers at chosen keypoints \*\*\*\*\*

ksel,s,kp,,1  
nslk,s  
\*get,nkp1,node,0,num,max       ! Retrieves a value and stores it as a scalar parameter or part of an array parameter\*\*\*\*\*  
nsl,all  
ksel,all

!ksel,s,kp,,2  
!nslk,s  
!\*get,nkp2,node,0,num,max       ! Retrieves a value and stores it as a scalar parameter or part of an array parameter\*\*\*\*\*  
!nsl,all  
!ksel,all

ksel,s,kp,,3  
nslk,s  
\*get,nkp3,node,0,num,max  
nsl,all  
ksel,all

ksel,s,kp,,5  
nslk,s

## Appendix B (Continued)

```
*get,nkp5,node,0,num,max
nset,all
kset,all
FINISH
```

```
!*****
!***** SOLUTION *****
!*****
```

```
/SOL
ANTYPE,0 ! Specifies the analysis type and restart status and "0" means
that it Performs a static analysis. Valid for all degrees of freedom
```

```
NLGEOM,1 ! Includes large-deflection effects in a static or full transient
analysis
```

```
!CNVTOL,U,,0.000001,,0
!CNVTOL,F,,0.0001,,0 ! Sets convergence values for nonlinear analyses
```

```
!*****
```

```
DK,1, ,0, , , ,UX,UY,UZ,ROTX,ROTZ,
```

```
DK,2, ,0, , , ,UY, , , , ,
```

```
!*****
```

```
loadsteps=800
*DO,step,1,loadsteps,1
theta=step*(.8*arclength)/loadsteps
```

```
!*****
```

```
DK,3,UZ,0
```

```
dispx=-(R-(R*cos(theta*PI/180)))
dispy=R*sin(theta*PI/180)
```

```
DK,3,UX,dispx
DK,3,UY,dispy
DK,3,ROTZ,theta*PI/180
LSWRITE,step
*ENDDO
LSSOLVE,1,loadsteps
```

## Appendix B (Continued)

/STATUS,SOLU

FINISH

!\*\*\*\*\*

!\*\*\*\*\* GET RESULTS \*\*\*\*\*

!\*\*\*\*\*

/POST1

\*DIM,rotY1, TABLE,loadSteps

\*DIM,fx1, TABLE,loadSteps ! Constrains: DK,1, ,0, , ,

,UX,UY,UZ,ROTX,ROTZ

\*DIM,fy1, TABLE,loadSteps

\*DIM,fz1, TABLE,loadSteps

\*DIM,mx1, TABLE,loadSteps

\*DIM,mz1, TABLE,loadSteps

\*DIM,fy2, TABLE,loadSteps ! Constrains: DK,2, ,0, , , ,UY, , , , ,

\*DIM,disX3, TABLE,loadSteps

\*DIM,disY3, TABLE,loadSteps

\*DIM,disZ3, TABLE,loadSteps

\*DIM,fz3, TABLE,loadSteps ! Constrains: DK,3,UZ,0

\*DIM,fx3, TABLE,loadSteps ! Constrains: DK,3,UX,dispx

\*DIM,fy3, TABLE,loadSteps ! Constrains: DK,3,UY,dispy

\*DIM,mz3, TABLE,loadSteps ! Constrains: DK,3,ROTZ,theta\*PI/180

\*DIM,disX5, TABLE,loadSteps

\*DIM,disY5, TABLE,loadSteps

\*DIM,disZ5, TABLE,loadSteps

\*Do,nn,1,loadSteps

set,nn

\*GET,roty,Node,nkp1,ROT,Y

\*SET,rotY1(nn),roty

\*GET,forcex,Node,nkp1,RF,FX

\*SET,fx1(nn),forcex

\*GET,forcey,Node,nkp1,RF,FY

\*SET,fy1(nn),forcey

\*GET,forcez,Node,nkp1,RF,FZ

\*SET,fz1(nn),forcez

\*GET,momx,Node,nkp1,RF,MX

\*SET,mx1(nn),momx

\*GET,momz,Node,nkp1,RF,MY

\*SET,mz1(nn),momz

## Appendix B (Continued)

\*GET,forcey,Node,nkp2,RF,Fy  
\*SET,fy2(nn),forcey

\*GET,disX,Node,nkp3,U,x  
\*SET,disX3(nn),disX  
\*GET,disY,Node,nkp3,U,Y  
\*SET,disY3(nn),disY  
\*GET,disz,Node,nkp3,U,Z  
\*SET,disZ3(nn),disz  
\*GET,forcez,Node,nkp3,RF,FZ  
\*SET,fz3(nn),forcez  
\*GET,forcey,Node,nkp3,RF,FY  
\*SET,fy3(nn),forcey  
\*GET,forcex,Node,nkp3,RF,FX  
\*SET,fx3(nn),forcex  
\*GET,momz,Node,nkp3,RF,MZ  
\*SET,mz3(nn),momz

\*GET,disX,Node,nkp5,U,x  
\*SET,disX5(nn),disX  
\*GET,disY,Node,nkp5,U,Y  
\*SET,disY5(nn),disY  
\*GET,disz,Node,nkp5,U,Z  
\*SET,disZ5(nn),disz

\*ENDDO

/output,output\_arc%arclength%\_asp%aspect%,txt,,Append

```
!*****  
!*****FILE HEADER: BEAM DATA*****  
!*****
```

\*MSG,INFO,'t','w','R','E','arclength','Iy2' ! Writes an output message via the  
ANSYS message subroutine. Max of 8 items per line  
%-14C %-10C %-10C %-10C %-10C %-8C

\*VWRITE,h2,b2,R,E2,arclength,Iy2 ! Writes data to a file in a formatted  
sequence. Max of 19 items per line  
%16.8G %-16.8G %-16.8G %-16.8G %-16.8G %-16.8G

```
!*****  
!*****DISPLACEMENT DATA SET*****  
!*****
```

**Appendix B (Continued)**

\*MSG,INFO,'roty1','disX3','disY3','disZ3','disX5','disY5','disZ5'  
%-10C %-10C %-8C %-8C %-8C %-8C %-8C

\*VWRITE,rotY1(1),disX3(1),disY3(1),disZ3(1),disX5(1),disY5(1),disZ5(1)  
% 16.8G %-16.8G %-16.8G %-16.8G %-16.8G %-16.8G %-16.8G

!\*\*\*\*\*  
!\*\*\*\*\*REACTIONS AT NODE 1\*\*\*\*\*  
!\*\*\*\*\*

\*MSG,INFO,'fx1','fy1','fz1','mx1','mz1'  
%-17C %-16C %-15C %-14C %-3C

\*VWRITE,fx1(1),fy1(1),fz1(1),mx1(1),mz1(1)  
% 16.8G %-16.8G %-16.8G %-16.8G %-16.8G

!\*\*\*\*\*  
!\*\*\*\*\*REACTIONS AT NODE 2\*\*\*\*\*  
!\*\*\*\*\*

\*MSG,INFO,'fy2'  
%-8C

\*VWRITE,fy2(1)  
% 16.8G

!\*\*\*\*\*  
!\*\*\*\*\*REACTIONS AT NODE 3\*\*\*\*\*  
!\*\*\*\*\*

\*MSG,INFO,'fz3','fx3','fy3','mz3'  
%-17C %-16C %-16C %-8C

\*VWRITE,fz3(1),fx3(1),fy3(1),mz3(1)  
% 16.8G % 16.8G % 16.8G % 16.8G

/output

FINISH

\*ENDDO  
\*ENDDO

## Appendix C: MATLAB code

```
%%%%%%%%%%%%%%%%%%%%%%%%%%%%%%%%%%%%%%%%%%%%%%%%%%%%%%%%%%%%%%%%%%%%%%%%%%
% Ansys data analysis file
% For an Ansys batch file
% which produces an output file
% Version 1: May 18,2007
% Version 2: June 7,2007
% Version 3: June 12, 2007
% Version 4: July 15, 2007
% Version 5: July 20, 2007
% Version 6: August 9, 2007
% Version 8: October 20, 2007
% Ansys Data File must provide: DATA
% rotation @ O: Y in column 1
% displacements @ Q: X,Y,Z in columns 2, 3 & 4 respectively
% displacement from A2 keypoint to D2 keypoint (more DA):
% X,Y,Z in columns 5,6,7
%%%%%%%%%%%%%%%%%%%%%%%%%%%%%%%%%%%%%%%%%%%%%%%%%%%%%%%%%%%%%%%%%%%%%%%%%%
clear all
R = 100; % radius of sphere = 100
arclength_v = 1:1:112; % define the vector of arclengths
%data_range = [2 2 2];
data_range = [112 110 98]; % Each aspect ratio has a
different ending data point so this range is needed
a_length = max(data_range);
asp=[0.1 0.4 0.7];
asp_length = length(asp);
CTHETA = zeros(a_length,asp_length);
CTHETA_check = zeros(a_length,asp_length);
GAMMA = zeros(a_length,asp_length);
CAPTHETA = zeros(a_length,asp_length);
KM = zeros(a_length,asp_length);
KF = zeros(a_length,asp_length);
P1 = zeros(a_length,asp_length);
P2 = zeros(a_length,asp_length);
P3 = zeros(a_length,asp_length);
P4 = zeros(a_length,asp_length);
CAPTHETA_MAX_M = zeros(a_length,asp_length);
CAPTHETA_MAX_F = zeros(a_length,asp_length);
CAPTHETA_MAX_FM = zeros(a_length,asp_length);
CAPTHETA_MAX = zeros(a_length,asp_length);
X = zeros(a_length,asp_length); % Number of data points W.R.T Beta
Y = zeros(a_length,asp_length); % Number of data points W.R.T Gamma
% assume a2 is a vector [ 0 5 0]
a2 = [0 5 0]; % a2 is length of y-frame vector at undeflected position
for i=1:asp_length,
    for counter=1:data_range(i),
        counter
        arclength = arclength_v(counter);
```

## Appendix C (Continued)

```
lambda = arclength*pi/180;

aspect=10*asp(i);
filename =
['output_arc',num2str(arclength),'_asp',num2str(aspect),'.txt'];
%string1 = 'C:\DOCUME~1\clusk2\800_Loadsteps\';
%Dr. Lusk's directory
string1 =
'C:\Docume~1\aleon2\Desktop\Work\Solution\1600_Loadsteps_ALL_8_9_07\';
% Working at school
%string1 =
'C:\Docume~1\Owner\Desktop\Solution\1600_Loadsteps_ALL\';
%Working at home
%string1 =
'C:\Docume~1\clusk2\MyDocu~1\Research\studen~1\AlexLe~1\800_Loadsteps\';
;
fid1 = fopen([string1,filename]); % opens the file
ABT = fread(fid1); % reads the file
into variable ABT in machine code
fclose(fid1); % closes the
data file
GBT = native2unicode(ABT); % changes data
from machine code to text and writes it to GBT
sB = findstr('Iy2',GBT); % finds end of
first header
sF = findstr('roty1',GBT); % finds
beginning of second header
s_iB = findstr('disZ5',GBT); % finds end of
first header
s_iF = findstr('fx1',GBT); % finds
beginning of second header
s_iB2 = findstr('mz1',GBT); % finds end of
second header
s_iF2 = findstr('fy2',GBT); % finds
beginning of third header
% s_iB3 = findstr('mz1',GBT); % finds end of
second header
s_iF3 = findstr('fz3',GBT); % finds
beginning of second header
s_iB3 = findstr('mz3',GBT);
header = str2num(GBT(sB(end)+4:sF(end)-1));
DATA = str2num(GBT(s_iB(end)+6:s_iF(end)-1)); % turns the
data into a numerical matrix
% DATA2 = str2num(GBT(s_iB2(end)+4:s_iF2(end)-1));
% gets the second chunk of data
% DATA3 = str2num(GBT(s_iF2(end)+4:s_iF3(end)-1));
DATA4 = str2num(GBT(s_iB3(end)+4:end));
D_size = size(DATA);
E = header(4);
Iy2 = header(6);
t = header(1);
w = header(2);
Iy1 = 1/12*w^3*t;
```

## Appendix C (Continued)

```

        phi_c    = DATA(:,1);           % phi is the
rotation of the rigid link in the X-Z plane about y
        beta_c   = atan2(DATA(:,3),R + DATA(:,2)); % beta is
defined by the displacement of point Q
%       fx1     = DATA2(:,1);
%       fy1     = DATA2(:,2);
%       fz1     = DATA2(:,3);
%       mx1     = DATA2(:,4);
%       mz1     = DATA2(:,5);
%       fy2     = DATA3;
%       fz3     = DATA4(:,1);
fx3_p    = DATA4(:,2);
fy3_p    = DATA4(:,3);
mz3_p    = DATA4(:,4);
%       fx3     = DATA4(:,2);
%       fy3     = DATA4(:,3);
%       mz3     = DATA4(:,4);
[pfx,sx] = polyfit(beta_c,fx3_p,15);
[pfy,sy] = polyfit(beta_c,fy3_p,15);
[pfz,sz] = polyfit(beta_c,mz3_p,15);
[fx3,dx3] = polyval(pfx,beta_c,sx);
[fy3,dy3] = polyval(pfy,beta_c,sy);
[mz3,dz3] = polyval(pfz,beta_c,sz);
fc1      = fx3.*cos(beta_c)+fy3.*sin(beta_c);
fc2      = -fx3.*sin(beta_c)+fy3.*cos(beta_c);
FC1(counter,i,:) = fc1*(lambda*R)^2/E/Iy2;
FC2(counter,i,:) = fc2*(lambda*R)^2/E/Iy2;
d2       = ones(D_size(1),1)*a2 +
[DATA(:,5),DATA(:,6),DATA(:,7)] - [DATA(:,2),DATA(:,3),DATA(:,4)];
mag_d2   = (d2(:,1).^2+d2(:,2).^2+d2(:,3).^2).^5;
da22    = d2(:,2)./mag_d2;
da23    = d2(:,3)./mag_d2;
theta0_c = atan2(da23,da22);
%       PHI(counter,i,:) = phi_c;
%       BETA(counter,i,:) = beta_c;
%       THETA0(counter,i,:) = theta0_c;
dgamma = .00005;
gamma_r = 0.75:dgamma:.9;
gamma   = ones(length(phi_c),1)*gamma_r;
beta    = beta_c *ones(1,length(gamma_r));
phi     = phi_c *ones(1,length(gamma_r));
theta0  = theta0_c *ones(1,length(gamma_r));
gamma_l = gamma*lambda;
%phi    =PHI(1,countBETA);
sincaptheta = sin(beta)./sin(gamma_l);
coscaptheta = tan((gamma_l-phi)).*cot(gamma_l);
captheta = atan2(sincaptheta,coscaptheta);
% epsilon_e is FEA based calculation of displacement vector
from the original
% to the final location of the end of the beam. It is
independent
% of the guess values for gamma.

```

## Appendix C (Continued)

```
abs_epsilon_e = sqrt((cos(beta).*cos(phi)-
ones(size(beta)).^2+(sin(beta)).^2+(cos(beta).*sin(phi)).^2); %
magnitude of vector epsilon_e
epsilon_ex = cos(beta).*cos(phi)-1; % x component of epsilon_e
epsilon_ey = sin(beta); % y component of epsilon_e
epsilon_ez = cos(beta).*sin(phi); % z component of epsilon_e
% epsilon_a is PRBM-based calculation of displacement vector
from the original
% to the final location of the end of the beam.
epsilon_ax = (cos(gamma_1)).^2.*(1-
cos(caphtheta))+cos(caphtheta)-1; % x component of epsilon_a
epsilon_ay = sin(caphtheta).*sin(gamma_1);
% y component of epsilon_a
epsilon_az = sin(gamma_1).*cos(gamma_1).(1-cos(caphtheta));
% z component of epsilon_a
error = sqrt((epsilon_ex-epsilon_ax).^2 +(epsilon_ey-
epsilon_ay).^2 +(epsilon_ez-epsilon_az).^2); % magnitude of vector
difference of epsilon_e and epsilon_a
rel_error = error./abs_epsilon_e;

% bool_rel_error is 1 if rel_error is less than .005
bool_rel_error = -1*floor(.5*(sign(rel_error)-.005));
d_bool = [zeros(1,length(gamma_r));diff(bool_rel_error)];
flag1 = 1-(cumsum(ceil(.5*d_bool)));
bool_rel_error_fixed = flag1.*bool_rel_error;
gamma_range_metric = sum(bool_rel_error_fixed);
[y,x]=max(gamma_range_metric);
Y(counter,i) = y;
X(counter,i) = x;

[c,h] = contour(rel_error,[0.005 0.005]);
drawnow
a = get(h,'ContourMatrix');
ax = a(1,:) - x;
ay = a(2,:) - y;
ai = find(abs(ax)<10);
[jumpsize, jumpspot] = max(diff(ai));
top_ax = ax(ai(1):ai(jumpspot));
top_ay = ay(ai(1):ai(jumpspot));
side_ax = ax(ai(jumpspot+1):ai(end));
side_ay = ay(ai(jumpspot+1):ai(end));
slope_side = diff(side_ay)./diff(side_ax);
[max_slope, max_slope_spot] = max(slope_side);
xa = side_ax(max_slope_spot); % adjustment to x
gamma_refine = xa*dgamma;
[ati_plus] = find(top_ax>xa);

ax1 = top_ax(ati_plus(1));
ay1 = top_ay(ati_plus(1));

[ati_minus] = find(top_ax<xa);
```

## Appendix C (Continued)

```
ax0 = top_ax(ati_minus(end));

ay0 = top_ay(ati_minus(end));
ya = (ay1-ay0)/(ax1-ax0)*(xa -ax0) + ay0 ; % adjustment to y

% y is index of the largest value of beta that gives a rel
error <
% .5%, x is the index of the best value of gamma
true_gamma = gamma_r(x) + gamma_refine; % best value of gamma
t_gamma_l = true_gamma*lambda;

% recalculate captheta with true gamma
d_beta = beta_c(y+1) - beta_c(y);
beta_refine = d_beta*ya;
d_phi = phi_c(y+1) -phi_c(y);
phi_refine = d_phi*ya;

true_sincaptheta = sin(beta_c)/sin(t_gamma_l);
true_coscapheta = tan((t_gamma_l-phi_c)).*cot(t_gamma_l);
capheta_v = atan2(true_sincaptheta,true_coscapheta);

sincaptheta_max = sin(beta_c(y)+beta_refine)/sin(t_gamma_l);
coscapheta_max = tan((t_gamma_l-
(phi_c(y)+phi_refine))).*cot(t_gamma_l);
capheta_max = atan2(sincaptheta_max,coscapheta_max);

% calculate forces/moments within short range
kf_t = (cos(capheta_v).*sin(t_gamma_l))./cos(beta_c).*((-
fx3*R.*sin(beta_c) + fy3*R.*cos(beta_c) ))./capheta_v;
km_t = (cos(capheta_v).*sin(t_gamma_l))./cos(beta_c).*((
mz3))./capheta_v;

km =
polyfit(capheta_v(1:end),km_t(1:end),0)*((lambda*R)/E/Iy2);
kf =
polyfit(capheta_v(1:end),kf_t(1:end),0)*((lambda*R)/E/Iy2);

km_theta = km/true_gamma;
kf_theta = kf/true_gamma;

KM(counter,i) = km;
KF(counter,i) = kf;
KMTHETA(counter,i,:) = km_theta;
KFTHETA(counter,i,:) = kf_theta;
FX3(counter,i,:) = fx3;
FY3(counter,i,:) = fy3;
MZ3(counter,i,:) = mz3;

%***** try to figure out fc1
f1 = fc1*(lambda*R)^3/E/Iy2;
```

## Appendix C (Continued)

```
[p,s] = polyfit(captheta_v(1:y),f1(1:y),3); % 3rd order fit
seems to work best
P1(counter,i) = p(1);
P2(counter,i) = p(2);
P3(counter,i) = p(3);
P4(counter,i) = p(4);

[yy,delta] = polyval(p,captheta_v,s);
%
% figure(1)
% plot(captheta_v*180/pi,[f1,y,y-delta,y+delta])
%
% %Ro = (f.^2/KR-2*R*f)/(2*KR*(1-cos(beta_c))-2*f);
% % rho = (R^2-2*R*Ro.*cos(beta_c)+Ro.^2).^0.5;
% %*****stress
% alpha_c = lambda-phi_c;
% sigma_x_f1 = fc1.*(-cos(beta_c).*sin(alpha_c))*(1/(t*w)-
R*w/(2*Iy1));
% sigma_x_f2 =
fc2.*sin(alpha_c).(sin(beta_c)/(t*w)+R*t/(2*Iy2)+R*w*sin(beta_c)/(2*I
y1));
% sigma_x_mz = mz3.*sin(alpha_c)*t/(2*Iy2);
% tau_xy_f2 = R*fc2.*(cos(alpha_c)-
cos(beta_c))/(.312*w*t^2);
% tau_xy_f1 = R*fc1.*sin(beta_c)/(.312*w*t^2);
% tau_xy_mz = mz3.*cos(alpha_c)/(.312*w*t^2);
% figure(3)
%
% plot(captheta_v*180/pi,[sigma_x_f1+sigma_x_f2+sigma_x_mz,sigma_x_f1,sig
ma_x_f2,sigma_x_mz])
% figure(2)
%
% plot(captheta_v*180/pi,[tau_xy_f1+tau_xy_f2+tau_xy_mz,tau_xy_f1,tau_xy_
f2,tau_xy_mz])
% tmax_f1 = (sigma_x_f1.^2+tau_xy_f1.^2).^0.5;
% tmax_f2 = (sigma_x_f2.^2+tau_xy_f2.^2).^0.5;
% tmax_mz = (sigma_x_mz.^2+tau_xy_mz.^2).^0.5;
% sigma_x = sigma_x_f1+sigma_x_f2+sigma_x_mz;
% tau_xy = tau_xy_f1+tau_xy_f2+tau_xy_mz;
% tmax = (sigma_x.^2+tau_xy.^2).^0.5;
% figure(3)
% plot(captheta_v*180/pi,tmax./(tmax_f2+tmax_mz)) % tmax is
the maxium shear stress including f1,f2& mz, f1 reduces the stress in
some cases.
% pause
% figure(1)
% hold on

%plot(captheta_v*180/pi,[km.*captheta_v,(cos(captheta_v).*sin(t_gamma_1
))./cos(beta_c).(mz3)*((lambda*R)/E/Iy2)])
% error_m = (km.*captheta_v-
((cos(captheta_v).*sin(t_gamma_1))./cos(beta_c).(mz3)*((lambda*R)/E/Iy
2)))./((cos(captheta_v).*sin(t_gamma_1))./cos(beta_c).(mz3)*((lambda*R
)/E/Iy2)));
```

## Appendix C (Continued)

```
%      M_error_m = [abs(error_m), abs(error_m)]
%      [c,h] = contour(M_error_m, [0.04 0.04])
%      a = get(h, 'ContourMatrix');
%      ay = a(2,:);
%      spot_m = max(ay);
%      ym = floor(spot_m);
%      incr = spot_m-ym;
%      d_capm = captheta_v(ym+1)-capheta_v(ym);
%      capheta_m_refine = incr*d_capm;
%      capheta_max_m = capheta_v(ym) +capheta_m_refine;
%      CAPTHETA_MAX_M(counter,i) = capheta_max_m;
%
%      % figure(2)
%      %hold on
%
%plot(capheta_v*180/pi, [kf.*capheta_v, (cos(capheta_v).*sin(t_gamma_1
)) ./cos(beta_c).*(fc2*R)*((lambda*R)/E/Iy2)])
%      error_f = (kf.*capheta_v-
((cos(capheta_v).*sin(t_gamma_1)) ./cos(beta_c).*(fc2*R)*((lambda*R)/E/
Iy2))) ./((cos(capheta_v).*sin(t_gamma_1)) ./cos(beta_c).*(fc2*R)*((lamb
da*R)/E/Iy2));
%      M_error_f = [abs(error_f), abs(error_f)]
%      [c,h] = contour(M_error_f, [0.04 0.04])
%      a = get(h, 'ContourMatrix');
%      ay = a(2,:);
%      spot_f = max(ay);
%      yf = floor(spot_f);
%      incr = spot_f-yf;
%      d_capf = capheta_v(yf+1)-capheta_v(yf);
%      capheta_f_refine = incr*d_capf;
%      capheta_max_f = capheta_v(yf) +capheta_f_refine;
%      CAPTHETA_MAX_F(counter,i) = capheta_max_f;

%figure(3)
% hold on

%plot(capheta_v*180/pi, [kf.*capheta_v, (cos(capheta_v).*sin(t_gamma_1
)) ./cos(beta_c).*(fc2*R)*((lambda*R)/E/Iy2)])
%      error_fm = ((kf+km).*capheta_v-
((cos(capheta_v).*sin(t_gamma_1)) ./cos(beta_c).*(fc2*R+mz3)*((lambda*R)
)/E/Iy2))) ./((cos(capheta_v).*sin(t_gamma_1)) ./cos(beta_c).*(fc2*R+mz3
))*((lambda*R)/E/Iy2));
%      M_error_fm = [abs(error_fm), abs(error_fm)]
%      [c,h] = contour(M_error_fm, [0.04 0.04])
%      a = get(h, 'ContourMatrix');
%      ay = a(2,:);
%      spot_fm = max(ay);
%      yfm = floor(spot_fm);
%      incr = spot_fm-yfm;
%      d_capfm = capheta_v(yfm+1)-capheta_v(yfm);
%      capheta_fm_refine = incr*d_capfm;
%      capheta_max_fm = capheta_v(yfm) +capheta_fm_refine;
%      CAPTHETA_MAX_FM(counter,i) = capheta_max_fm;
```

## Appendix C (Continued)

```
%CAPTHETA_MAX(counter,i) = captheta_v(end);

% k_resol = (((km+kf).*captheta_v) -
((cos(captheta_v).*sin(t_gamma_1))./cos(beta_c).*(fc2*R+mz3)*((lambda*R)/E/Iy2)))./((cos(captheta_v).*sin(t_gamma_1))./cos(beta_c).*(fc2*R+mz3))*((lambda*R)/E/Iy2));
%min_k = min(k);
% min_k = 1.5/((lambda*R)/E/Iy2);
% max_k = 2.5/((lambda*R)/E/Iy2);
% %max_k = max(k);
% dk = (max_k-min_k)./1000;
% K_r = [min_k:dk:max_k];
% fx_m = fx3*ones(size(K_r));
% fy_m = fy3*ones(size(K_r));
% mz_m = mz3*ones(size(K_r));
% beta_m = beta_c*ones(size(K_r));
% captheta_m = captheta(:,x)*ones(size(K_r));
% K_m = ones(size(fx3))*K_r;
% error2 = fx_m.*(-
R*tan(beta_m).*cos(captheta_m)*sin(t_gamma_1)) +
fy_m.*(R*cos(captheta_m)*sin(t_gamma_1)) +
mz_m.*cos(captheta_m)./cos(beta_m).*sin(t_gamma_1)-K_m.*captheta_m;
% tv = fx_m.*(-R*tan(beta_m).*cos(captheta_m).*sin(t_gamma_1))
+ fy_m.*(R*cos(captheta_m).*sin(t_gamma_1)) +
mz_m.*cos(captheta_m)./cos(beta_m).*sin(t_gamma_1);
% rel_error2 = abs(error2./tv);
%
% bool_rel_error2 = -1*floor(.5*(sign(rel_error2-.05)));
% d_bool2 = [zeros(1,length(K_r));diff(bool_rel_error2)];
% %flag2 = 1-(cumsum(ceil(.5*d_bool2)));
% %bool_rel_error_fixed2 = flag2.*bool_rel_error2;
% %K_range_metric2 = sum(bool_rel_error_fixed2);
% K_range_metric2 = sum(bool_rel_error2);
% [y2,x2]=max(K_range_metric2);
% Y2(counter,i) = y2;
% X2(counter,i) = x2;
% true_k = K_r(x2)*(lambda*R)/E/Iy2
% %k_nd = k*lambda*R/E/Iy2; % nondimensional form of k
% %KND(counter,i,:) = [k_nd;1./zeros(length(beta_c)-y,1)];
% figure(4)
% clf
% % [c,h]=contour(captheta*180/pi,gamma,rel_error,[0:.01:.05])
% pcolor(captheta_m*180/pi,K_m,bool_rel_error2),shading
flat,colorbar('horiz')
% %clabel(c,h)
% title(['\lambda = ',num2str(lambda*180/pi)])
% %
% % figure(5)
% %
% % clf
% %
% % % [c,h]=contour(captheta*180/pi,gamma,rel_error,[0:.01:.05])
% %
% % pcolor(captheta_m*180/pi,K_m,bool_rel_error_fixed2),shading flat
% %
% % %clabel(c,h)
% %
% % drawnow
% %
% % figure(6)
```

## Appendix C (Continued)

```
%      clf
%      %[c,h]=contour(beta,gamma,rel_error,[0:.01:.05])
%      %plot(short_capheta*180/pi,short_theta0_c*180/pi)
%      % plot(short_capheta*180/pi,k_nd)
%      plot(beta_c,[dx3,dy3,dz3]);
%      %clabel(c,h)
%      drawnow
%      %pause
%      [p2,s2] = polyfit(capheta_v(1:y),theta0_c(1:y),1);
%      CTHETA(counter,i)      = p2(1);
%      CTHETA_check(counter,i) = p2(2);
%      GAMMA(counter,i)      = true_gamma;
%      CAPTHETA(counter,i)   = capheta_max*180/pi;
%
end
%      figure(1)
%      plot(squeeze(PHI(counter, :, :))*180/pi)
%      title(['arclength = ', num2str(arclength)])
%      xlabel('loadsteps')
%      ylabel('\phi')
%      leg_matrix = []; % create
legend matrix
%      for i = 1:asp_length
%          leg_matrix = [leg_matrix; 'aspect ratio = ', num2str(asp(i))];
%      end
%      legend(leg_matrix, 'Location', 'Best')
%      figure(2)
%      plot(squeeze(BETA(counter, :, :))*180/pi)
%      title(['arclength = ', num2str(arclength)])
%      xlabel('loadsteps')
%      ylabel('\beta')
%      leg_matrix = []; % create
legend matrix
%      for i = 1:asp_length
%          leg_matrix = [leg_matrix; 'aspect ratio = ', num2str(asp(i))];
%      end
%      legend(leg_matrix, 'Location', 'Best')
%      figure(3)
%      plot(squeeze(THETA0(counter, :, :))*180/pi)
%      title(['arclength = ', num2str(arclength)])
%      xlabel('loadsteps')
%      ylabel('\theta_0')
%      leg_matrix = []; % create
legend matrix
%      for i = 1:asp_length
%          leg_matrix = [leg_matrix; 'aspect ratio = ', num2str(asp(i))];
%      end
%      legend(leg_matrix, 'Location', 'Best')
%      pause
end

[P1_asp1_fit,s11] =
polyfit(arclength_v(1:data_range(1))',P1(1:data_range(1),1),5);
```

## Appendix C (Continued)

```
[P1_asp4_fit,s12] =  
polyfit(arclength_v(1:data_range(2))',P1(1:data_range(2),2),5);  
[P1_asp7_fit,s13] =  
polyfit(arclength_v(1:data_range(3))',P1(1:data_range(3),3),5);  
[P1_1_y,P1_delta_1] = polyval(P1_asp1_fit,arclength_v,s11);  
[P1_2_y,P1_delta_2] = polyval(P1_asp4_fit,arclength_v,s12);  
[P1_3_y,P1_delta_3] = polyval(P1_asp7_fit,arclength_v,s13);
```

```
[P2_asp1_fit,s21] =  
polyfit(arclength_v(1:data_range(1))',P2(1:data_range(1),1),5);  
[P2_asp4_fit,s22] =  
polyfit(arclength_v(1:data_range(2))',P2(1:data_range(2),2),5);  
[P2_asp7_fit,s23] =  
polyfit(arclength_v(1:data_range(3))',P2(1:data_range(3),3),5);  
[P2_1_y,P2_delta_1] = polyval(P2_asp1_fit,arclength_v,s21);  
[P2_2_y,P2_delta_2] = polyval(P2_asp4_fit,arclength_v,s22);  
[P2_3_y,P2_delta_3] = polyval(P2_asp7_fit,arclength_v,s23);
```

```
[P3_asp1_fit,s31] =  
polyfit(arclength_v(1:data_range(1))',P3(1:data_range(1),1),5);  
[P3_asp4_fit,s32] =  
polyfit(arclength_v(1:data_range(2))',P3(1:data_range(2),2),5);  
[P3_asp7_fit,s33] =  
polyfit(arclength_v(1:data_range(3))',P3(1:data_range(3),3),5);  
[P3_1_y,P3_delta_1] = polyval(P3_asp1_fit,arclength_v,s31);  
[P3_2_y,P3_delta_2] = polyval(P3_asp4_fit,arclength_v,s32);  
[P3_3_y,P3_delta_3] = polyval(P3_asp7_fit,arclength_v,s33);
```

```
[P4_asp1_fit,s41] =  
polyfit(arclength_v(1:data_range(1))',P4(1:data_range(1),1),5);  
[P4_asp4_fit,s42] =  
polyfit(arclength_v(1:data_range(2))',P4(1:data_range(2),2),5);  
[P4_asp7_fit,s43] =  
polyfit(arclength_v(1:data_range(3))',P4(1:data_range(3),3),5);  
[P4_1_y,P4_delta_1] = polyval(P4_asp1_fit,arclength_v,s41);  
[P4_2_y,P4_delta_2] = polyval(P4_asp4_fit,arclength_v,s42);  
[P4_3_y,P4_delta_3] = polyval(P4_asp7_fit,arclength_v,s43);
```

```
% for i = 1:asp_length  
%     figure(1)  
%     plot(squeeze(PHI(:,i,:))'*180/pi)  
%     title(['aspect ratio = ',num2str(asp(i))])  
%     xlabel('loadsteps')  
%     ylabel('\phi')  
%     leg_matrix = []; % create legend matrix  
%     if a_length<10,  
%         for counter =1:a_length  
%             leg_matrix = [leg_matrix;'arc =  
' ,num2str(arclength_v(counter))];  
%         end
```

## Appendix C (Continued)

```
%         legend(leg_matrix,'Location','Best')
%     end
%     figure(2)
%     plot(squeeze(BETA(:,i,:))'*180/pi)
%     title(['aspect ratio = ',num2str(asp(i))])
%     xlabel('loadsteps')
%     ylabel('\beta')
%     leg_matrix = []; % create legend matrix
%     if a_length<10
%         for counter =1:a_length
%             leg_matrix = [leg_matrix;'arc =
',num2str(arclength_v(counter))];
%         end
%         legend(leg_matrix,'Location','Best')
%     end
%     figure(3)
%     plot(squeeze(THETA0(:,i,:))'*180/pi)
%     title(['aspect ratio = ',num2str(asp(i))])
%     xlabel('loadsteps')
%     ylabel('\theta_0')
%     leg_matrix = []; % create legend matrix
%     if a_length<10,
%         for counter =1:a_length
%             leg_matrix = [leg_matrix;'arc =
',num2str(arclength_v(counter))];
%         end
%         legend(leg_matrix,'Location','Best')
%     end
%
%     pause
% end

% C_M = squeeze(MZ3)./squeeze(FC2);
flag1 = sign(GAMMA);
figure(1)
plot(arclength_v,GAMMA./flag1)
xlabel('\lambda, (deg)')
ylabel('\gamma')
legend('Asp_{0.1}','Asp_{0.4}','Asp_{0.7}','Location','NorthEastOutside
')
print gamma -dtiff -r600
print gamma -dps -r600

figure(2)
plot(arclength_v,CTHETA./flag1)
xlabel('\lambda, (deg)')
ylabel('c_{\theta}')
legend('Asp_{0.1}','Asp_{0.4}','Asp_{0.7}','Location','NorthEastOutside
')
print ctheta -dtiff -r600
print ctheta -dps -r600
```

## Appendix C (Continued)

```
% figure(2)
% plot(arclength_v,CTHETA_check)

figure(3)
plot(arclength_v,CAPTHETA./flag1)
xlabel('\lambda, (deg)')
ylabel('\Theta (\gamma), (deg)')
legend('Asp_{0.1}','Asp_{0.4}','Asp_{0.7}','Location','NorthEastOutside')
print captheta_g -dtiff -r600
print captheta_g -dps -r600

figure(4)
plot(arclength_v,[KM'./flag1';KF'./flag1'])
xlabel('\lambda, (deg)')
ylabel('K_m, K_f')
legend('K_m Asp_{0.1}','K_m Asp_{0.4}','K_m Asp_{0.7}','K_f Asp_{0.1}','K_f Asp_{0.4}','K_f Asp_{0.7}','Location','NorthEastOutside')
print KmKf -dtiff -r600
print KmKf -dps -r600

figure(5)
plot(arclength_v,[P1'./flag1';[P1_1_y;P1_2_y;P1_3_y]./flag1'])
xlabel('\lambda, (deg)')
ylabel('P_1')
legend('Data Asp_{0.1}','Data Asp_{0.4}','Data Asp_{0.7}','Curve Fit Asp_{0.1}','Curve Fit Asp_{0.4}','Curve Fit Asp_{0.7}','Location','NorthEastOutside')
print P1 -dtiff -r600
print P1 -dps -r600

figure(6)
plot(arclength_v,[P2'./flag1';[P2_1_y;P2_2_y;P2_3_y]./flag1'])
xlabel('\lambda, (deg)')
ylabel('P_2')
legend('Data Asp_{0.1}','Data Asp_{0.4}','Data Asp_{0.7}','Curve Fit Asp_{0.1}','Curve Fit Asp_{0.4}','Curve Fit Asp_{0.7}','Location','NorthEastOutside')
print P2 -dtiff -r600
print P2 -dps -r600

figure(7)
plot(arclength_v,[P3'./flag1';[P3_1_y;P3_2_y;P3_3_y]./flag1'])
xlabel('\lambda, (deg)')
ylabel('P_3')
legend('Data Asp_{0.1}','Data Asp_{0.4}','Data Asp_{0.7}','Curve Fit Asp_{0.1}','Curve Fit Asp_{0.4}','Curve Fit Asp_{0.7}','Location','NorthEastOutside')
```

## Appendix C (Continued)

```
print P3 -dtiff -r600
print P3 -dps -r600

figure(8)
plot(arclength_v,[P4'./flag1';[P4_1_y;P4_2_y;P4_3_y]./flag1'])
xlabel('\lambda, (deg)')
ylabel('P_4')
legend('Data Asp_{0.1}','Data Asp_{0.4}','Data Asp_{0.7}','Curve Fit
Asp_{0.1}','Curve Fit Asp_{0.4}','Curve Fit
Asp_{0.7}','Location','NorthEastOutside')
print P4 -dtiff -r600
print P4 -dps -r600

% figure(5)
% plot(arclength_v,P1)
%
% figure(6)
% plot(arclength_v,P2)
%
% figure(7)
% plot(arclength_v,P3)
%
% figure(8)
% plot(arclength_v,P4)

% figure(9)
% plot(arclength_v,CAPTHETA_MAX_M*180/pi./flag1)
%
% figure(10)
% plot(arclength_v,CAPTHETA_MAX_F*180/pi./flag1)

figure(11)
plot(arclength_v,CAPTHETA_MAX_FM*180/pi./flag1)
xlabel('\lambda, (deg)')
ylabel('\Theta (K), (deg)')
legend('Asp_{0.1}','Asp_{0.4}','Asp_{0.7}','Location','NorthEastOutside
')
print capthetaK -dtiff -r600
print capthetaK -dps -r600

figure (12)
plot(captheta_v*180/pi,squeeze(FC1([1,20,45,90,110],1,:)))
xlabel('\Theta, (deg)')
ylabel('F_{c1}')
title('For aspect ratio 0.1')
text(75,-0.1,'\lambda=1')
text(65,0.35,'\lambda=20')
text(35,0.3,'\lambda=45')
text(81,4,'\lambda=90')
text(81.16,2.375,'\lambda=110')
print ForceC1_aps1 -dtiff -r600
```

## Appendix C (Continued)

```
print ForceC1_asp1 -dps -r600
```

```
figure (13)
plot(captheta_v*180/pi, squeeze(FC1([1,20,45,90,110],2,:)))
xlabel('\Theta, (deg)')
ylabel('F_{c1}')
title('For aspect ratio 0.4')
text(75,-0.1, '\lambda=1')
text(79.32,1.184, '\lambda=20')
text(65.22,0.9737, '\lambda=45')
text(80.77,4.395, '\lambda=90')
text(80.15,2.254, '\lambda=110')
print ForceC1_asp4 -dtiff -r600
print ForceC1_asp4 -dps -r600
```

```
figure (14)
plot(captheta_v*180/pi, squeeze(FC1([1,20,45,90,110],3,:)))
xlabel('\Theta, (deg)')
ylabel('F_{c1}')
title('For aspect ratio 0.7')
text(75.38,0.2588, '\lambda=1')
text(78.08,1.18, '\lambda=20')
text(80.56,3.186, '\lambda=45')
text(80.77,5.007, '\lambda=90')
text(73.1, -0.1506, '\lambda=110')
print ForceC1_asp7 -dtiff -r600
print ForceC1_asp7 -dps -r600
```

## Appendix D: Napier's rule for spherical triangles

### Spherical Triangles

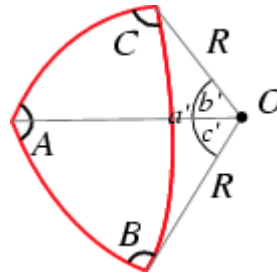


Figure D-1: Spherical triangles

A spherical triangle is a figure formed on the surface of a sphere by three great circular arcs intersecting pair-wise in three vertices. The spherical triangle is the spherical analog of the planar triangle, and is sometimes called an Euler triangle [32]. Let a spherical triangle have angles  $A$ ,  $B$ , and  $C$  (measured in radians at the vertices along the surface of the sphere) and let the sphere on which the spherical triangle sits have radius  $R$  [32]

### Napier Rules

Napier's rules are used to derive the parameters required to analyze the bending of curved beam. The derivation of parameters can be easily obtained from two simple rules discovered by John Napier (1550-1617), the inventor of logarithms.

(<http://www.angelfire.com/nt/navtrig/B2.html>). As the right angle does not enter into the

## Appendix D (Continued)

formulas, only five parts are considered. These are  $a$ ,  $b$ , and the complements of  $A$ ,  $B$ , and  $C$  (or  $90-A$ ,  $90-B$ ,  $90-c$ ) which can be written  $A'$ ,  $B'$ , and  $c'$ . If these five parts are arranged in the order in which they occur in the triangle, any part may be selected and called the middle part; then the two parts next to it are called adjacent parts, and the other two are called opposite parts.

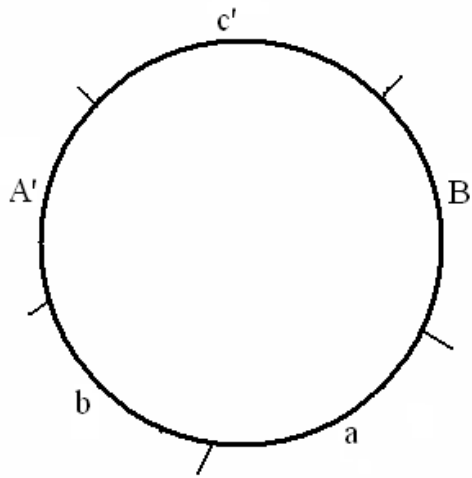


Figure D-2: Five parts arranged in order of occurrence

Napier's rules are as follows:

1. The sine of the middle part equals the product of the tangents of the adjacent parts.
2. The sine of the middle part equals the product of the cosines of the opposite parts.

The right spherical triangle for the PRBM has the sides,  $\gamma\lambda$ ,  $\beta$ ,  $\eta$ . The right angle lies between the 'sides'  $\beta$  and  $\eta$ .  $\Theta$  is the pseudo-rigid-body angle.  $\eta'$  is the angle opposite to  $\eta$  as shown in Figure D-3

Appendix D (Continued)

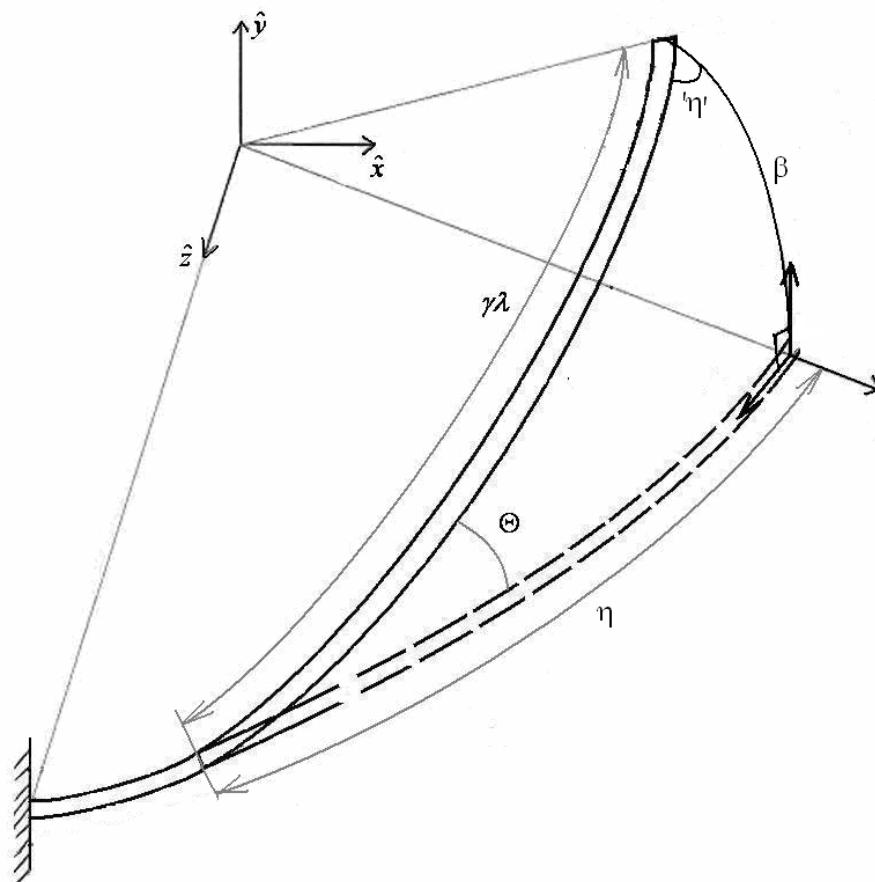


Figure D-3: Spherical right triangle

## Appendix D (Continued)

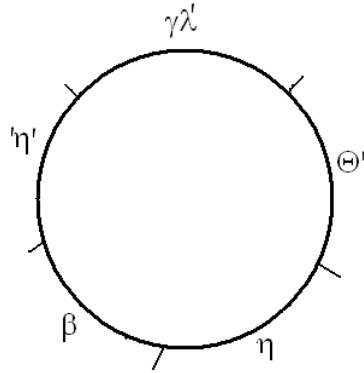


Figure D-4: Five parts for PRBM right spherical triangle.

Using Napier Rules the following equations can be obtained.

$$\sin(90 - \Theta) = \tan \eta \tan(90 - \Theta)$$

Where  $\eta = (\lambda - \phi) - (\lambda - \gamma\lambda)$

and  $\alpha = \lambda - \phi$

To get

$$\Theta = \tan^{-1} \left[ \frac{\tan \beta}{\sin[\alpha - \lambda(1 - \gamma)]} \right]$$

## Appendix D (Continued)

At  $\beta=90^\circ$  this equation fails to give a value of pseudo-rigid body angle  $\Theta$  to overcome this,  $\Theta$  is also expressed in an alternate form. From Napier Rules we get

$$\sin \Theta = \frac{\sin \beta}{\sin \gamma \lambda}$$

and

$$\cos \Theta = \tan \eta \cot \gamma \lambda$$

To get

$$\Theta = \tan^{-1} \left[ \frac{\sin \beta / \sin \gamma \lambda}{\tan \eta \cot \gamma \lambda} \right]$$